Khaled M. Elsayes
Editor

Cross-Sectional Imaging of the Abdomen and Pelvis

A Practical Algorithmic Approach

Springer

Cross-Sectional Imaging of the Abdomen and Pelvis

Khaled M. Elsayes
Editor

Cross-Sectional Imaging of the Abdomen and Pelvis

A Practical Algorithmic Approach

Springer

Editor
Khaled M. Elsayes, MD
Department of Diagnostic Radiology
The University of Texas MD Anderson Cancer Center
Houston, TX, USA

ISBN 978-1-4939-1883-6 ISBN 978-1-4939-1884-3 (eBook)
DOI 10.1007/978-1-4939-1884-3
Springer New York Heidelberg Dordrecht London

Library of Congress Control Number: 2015934697

Printed on acid-free paper

Springer is part of Springer Science+Business Media (www.springer.com)

To the memory of my parents
To my wife and children

Preface

The continuing advancements in cross-sectional imaging of the abdomen and pelvis have significantly increased the complexity of this field. Our book is written as an alternative to the traditionally large (and hard to learn) reference textbooks. In simple words, radiologists should attempt to learn the essentials first and then delve into the in-depth concepts. This up-to-date book contains practical and concise descriptions, high-quality illustrations, and state-of-the-art techniques, with a discussion of the most common clinical cases encountered in daily practice.

The book is different from current radiology teaching books as it presents diagnoses from a practical point of view. Most of the current radiology books discuss various diseases and classify them from the pathology standpoint. Our book derives the cases from the radiology reading room and uses an algorithmic approach to help make a working differential diagnosis and reach an accurate diagnosis based on imaging features, considering clinical, laboratory, and other underlying contexts.

The book is written with practicing radiologists and radiology residents in mind. We discuss typical and atypical radiological manifestations that step the reader through a radiologist's analysis of these patterns. The cases are presented progressively, with the expert's thinking process described in detail. Comments at the end tie up loose ends and provide references and additional relevant factual material. Algorithms are provided to demonstrate the diagnostic approach and enforce the knowledge.

This book is divided into several chapters according to anatomical organ of origin. We start each chapter with a brief anatomical background and practical notes about the utility of various cross-sectional imaging techniques. The most common pathologies are then listed, followed by practical algorithms based on frequently encountered imaging features. A pictorially relevant discussion of pertinent pathologies is offered.

Special emphasis is placed predominantly on the role of computed tomography (CT) and magnetic resonance imaging (MRI). A more focused discussion of the role of ultrasound (US) is covered when US is utilized as an imaging modality of choice (e.g., in the evaluation of organ transplant).

In addition to simple practical algorithmic coverage of many pathological entities in various abdominopelvic organs, unique topics are also illustrated such as imaging of organ transplant (including kidney, liver, and pancreas), evaluation of perianal fistula, and evaluation of rectal carcinoma and prostate carcinoma by MRI. Brief overviews are also included to simplify understanding of specific techniques such as dual energy, CT enterography, and virtual colonoscopy.

Based on the effect of similar material we use with our residents and fellows, I believe that the practical emphasis of this text will be useful to radiology residents, fellows, and practicing radiologists wishing to learn about cross-sectional imaging of the abdomen and pelvis in a simple and practical algorithmic approach. However, it should be noted that although these algorithms help in making a correct differential diagnosis in most cases, there can be exceptions of the rule, which are especially noted with rare cases.

Houston, TX, USA — Khaled M. Elsayes, MD

Acknowledgements

First and foremost, I would like to thank the Almighty God, who has guided me to learn this knowledge

I also take this opportunity to extend my appreciation to those individuals who have been instrumental in my career in radiology and those who have inspired me to complete this project

To my mentors, friends and all colleagues in:

- MD Anderson Cancer Center, especially, Chusilp Charnsangavej and Marshall Hicks
- University of Michigan, especially, Isaac Francis, Joel Platt, James Ellis, Rich Cohan and Hero Hussain
- Egypt, especially, Hazem Moharram, Mamdouh Mahfouz, Tarek Eldiasty, Ikram Hamed, Ahmed Samy, Mohamed Moustafa, Moustafa Ismail, Omar Moawyah, Ihab Fathy and Amr Nasef
- Mallinckrodt Institute of Radiology, especially, Jeffrey J. Brown, Vamsidhar R. Narra, Jay Heiken and Christine Menias
- Elsewhere, especially, John Leyendecker (Wake Forest), Rich Baron (Chicago), Haitham Elsamalouty (Toledo) and Akram Shaaban (Utah)

To all contributors of this book

To the great medical illustrator, David Bier

To all of my medical students and residents

Contents

Contributors

Ahmed Abdelbaki, MBBCh Department of Surgery, Guthrie Robert Packer Hospital, Sayre, PA, USA

Diego A. Aguirre, MD Department of Radiology and Medical Imaging, Fundación Santa Fe de Bogotá University Hospital, Bogota, Colombia

Kareem Ahmed, MD Department of Diagnostic Radiology, The University of Texas MD Anderson Cancer Center, Houston, TX, USA

Mohammed S. Al-Natour, MD Department of Diagnostic Radiology, University of Toledo, Toledo, OH, USA

Ahmed M. Amer, MD Department of Diagnostic Radiology, The University of Texas MD Anderson Cancer Center, Houston, TX, USA

Mohamed K. Asran, MD Department of Diagnostic Imaging, National Cancer Institute, Cairo University, Cairo, Egypt

Richard L. Baron, MD Department of Radiology, University of Chicago Medical Center, Chicago, IL, USA

Stuart Bentley-Hibbert, MD, PhD Department of Radiology, Columbia University Medical Center, New York, NY, USA

Senta M. Berggruen, MD Department of Radiology, Northwestern Memorial Hospital, Chicago, IL, USA

Priya R. Bhosale, MD Department of Diagnostic Radiology, The University of Texas MD Anderson Cancer Center, Houston, TX, USA

Juan C. Camacho, MD Abdominal Imaging Division and Division of Interventional Radiology and Image-guided Medicine, Emory University School of Medicine, Atlanta, GA, USA

Department of Radiology and Imaging Sciences, Emory University School of Medicine, Atlanta, GA, USA

Vinika Chaudhari, MD Department of Radiological Sciences, Ronald Reagan UCLA Medical Center, Los Angeles, CA, USA

Anil Chauhan, MD Department of Abdominal Imaging, Department of Radiology, University of Pennsylvania, Philadelphia, PA, USA

Adam Culverwell, MBChB, FRCR Department of Clinical Radiology, Harrogate Hospital, Harrogate, North Yorkshire, UK

Department of Clinical Radiology, Lincoln Wing, St. James's University Hospital, Leeds, UK

Michael R. Da Rosa, MD Department of Medical Imaging, University of Toronto, Toronto, ON, Canada

Sandeep P. Deshmukh, MD Department of Radiology, Thomas Jefferson University Hospital, Philadelphia, PA, USA

Jonathan R. Dillman, MD Department of Radiology, University of Michigan Health System, Ann Arbor, MI, USA

Yehia Mostafa Elguindy, MD Department of Diagnostic Radiology, University of Toledo Medical Center, Toledo, OH, USA

Haitham Elsamaloty, MD Department of Diagnostic Radiology, University of Toledo Medical Center, Toledo, OH, USA

Khaled M. Elsayes, MD Department of Diagnostic Radiology, The University of Texas MD Anderson Cancer Center, Houston, TX, USA

Randy D. Ernst, MD Department of Diagnostic Imaging, The University of Texas MD Anderson Cancer Center, Houston, TX, USA

Ayman H. Gaballah, MD, FRCR Department of Radiology, University of Michigan, Ann Arbor, MI, USA

Karthik Ganesan, MBBS, DNB Department of 3 T F-MRI, SRL Diagnostics – Jankaria Imaging, Mumbai, India

Dhakshina Moorthy Ganeshan, MD Department of Diagnostic Radiology, The University of Texas MD Anderson Cancer Center, Houston, TX, USA

Ajit H. Goenka, MD Department of Abdominal Imaging, Cleveland Clinic, Cleveland, OH, USA

Shiva Gupta, MD Department of Diagnostic Radiology, The University of Texas MD Anderson Cancer Center, Houston, TX, USA

Masoom A. Haider, MD, FRCP(C) Department of Medical Imaging, University of Toronto, Toronto, ON, Canada

Department of Medical Imaging, Sunnybrook Health Sciences Centre, Toronto, ON, Canada

Hero K. Hussain, MD Department of Diagnostic Radiology, University of Michigan Health Center, Ann Arbor, MI, USA

Rachel Hyland, MBChB, FRCR Department of Clinical Radiology, St. James's University Hospital, Leeds Teaching Hospitals NHS Trust, Leeds, West Yorkshire, UK

Juan J. Ibarra-Rovira, MD Department of Diagnostic Radiology, Baylor College of Medicine, Houston, TX, USA

Yassine Kanaan, MD Department of Radiology, Texas Scottish Rite Hospital for Children, Dallas, TX, USA

Devaraju Kanmaniraja, MD Department of Radiology, Cleveland Clinic Hospital, Cleveland, OH, USA

Department of Abdominal Imaging, Cleveland Clinic, Cleveland, OH, USA

Harmeet Kaur, MD Department of Diagnostic Imaging, The University of Texas MD Anderson Cancer Center, Houston, TX, USA

Ott Le, MD Department of Diagnostic Radiology, The University of Texas MD Anderson Cancer Center, Houston, TX, USA

Ravinder S. Legha, MD Department of Diagnostic Imaging, The University of Texas MD Anderson Cancer Center, Houston, TX, USA

Leonardo P. Marcal, MD Department of Diagnostic Radiology, The University of Texas MD Anderson Cancer Center, Houston, TX, USA

Eduardo J. Matta, MD Department of Diagnostic and Interventional Imaging, University of Texas, Houston, Houston, TX, USA

Christine O. Menias, MD Department of Radiology, Mallinckrodt Institute of Radiology, St. Louis, MO, USA

Ajaykumar C. Morani, MBBS, DNB, MD, DABR Department of Radiology, The University of Texas MD Anderson Cancer Center, Houston, TX, USA

Courtney Coursey Moreno, MD Department of Radiology and Imaging Sciences, Emory Healthcare, Emory University School of Medicine, Atlanta, GA, USA

Ricardo D. Moreno, MD Department of Surgery, The Southeast Permanente Medical Group, Kaiser Permanente, Atlanta, GA, USA

Shalini Vicky Mukhi, MD Department of Radiology, Baylor College of Medicine/Michael E. Debakey VA Medical Center, Houston, TX, USA

Sherif G. Nour, MD, FRCR Department of Radiology and Imaging Sciences, Emory University Hospitals and School of Medicine, Atlanta, GA, USA

Maitraya K. Patel, MD Department of Radiology, Olive View – UCLA Medical Center, Sylmar, CA, USA

Joel F. Platt, MD Department of Radiology, University of Michigan, Ann Arbor, MI, USA

Anand M. Prabhakar, MD Department of Radiology, Massachusetts General Hospital, Boston, MA, USA

Hima B. Prabhakar, MD Department of Radiology, Perelman School of Medicine at the University of Pennsylvania, Philadelphia, PA, USA

Steven S. Raman, MD Department of Radiology, Ronald Reagan UCLA Medical Center, David Geffen School of Medicine at UCLA, Los Angeles, CA, USA

Kathleen Ruchalski, MD Department of Radiology, Ronald Reagan UCLA Medical Center, Los Angeles, CA, USA

Laura Elizabeth Traube, MD, MPH Department of Radiology, Ronald Reagan UCLA Medical Center, Los Angeles, CA, USA

Tara Sagebiel, MD Department of Diagnostic Radiology, The University of Texas MD Anderson Cancer Center, Houston, TX, USA

Akram M. Shaaban, MBBCh Department of Radiology, University of Utah Medical Center, Salt Lake City, UT, USA

Shetal N. Shah, MD Department of Radiology, Cleveland Clinic Hospital, Cleveland, OH, USA

Imaging Institute, Cleveland Clinic, Cleveland, OH, USA

Haiyham M. Shebel, MD Department of Radiology, Urology and Nephrology Center, Mansoura University, Mansoura, Egypt

Nasir Siddiqui, MD Department of Radiology, Riverside Memorial Hospital, Columbus, OH, USA

Janio Szkarluk, MD, PhD Department of Diagnostic Radiology, The University of Texas MD Anderson Cancer Center, Houston, TX, USA

Damian J. M. Tolan, MBChB, FRCR Department of Clinical Radiology, Lincoln Wing, St. James's University Hospital, Leeds, UK

Keith P. Tomich, MD Department of Radiology, Kaiser Permanente Georgia Region, Atlanta, GA, USA

Hüseyin Gürkar Töre, MD Department of Radiology, Northwestern University-Feinberg School of Medicine, Chicago, IL, USA

David J. Vining, MD Department of Radiology, The University of Texas MD Anderson Cancer Center, Houston, TX, USA

Nicolaus A. Wagner-Bartak, MD Department of Diagnostic Imaging, The University of Texas MD Anderson Cancer Center, Houston, TX, USA

Ashish P. Wasnik, MD Department of Radiology, University of Michigan Health System, Ann Arbor, MI, USA

Vahid Yaghmai, MD Department of Radiology, Northwestern University-Feinberg School of Medicine, Chicago, IL, USA

Ehab Youssef, MD, FRCR Department of Radiology, University of Michigan, Ypsilanti, MI, USA

Overview of CT and MRI Techniques of the Liver

1

Tara Sagebiel and Janio Szkarluk

Computed Tomography

The widespread availability, cost, and speed of exam make computed tomography (CT) the most common modality used to evaluate the liver. Modern CT scanners image the entire liver during multiple phases of contrast enhancement, providing enhancement information important to lesion characterization. CT's high spatial resolution can produce detailed multiplanar reconstruction images that can clarify the segmental location of a hepatic lesion and a lesion's relationship to the hepatic vasculature, biliary tree, and extrahepatic structures. CT can also calculate the future liver remnant (FLR) and future liver volume (FLV) making CT an important tool in presurgical planning.

Non-contrast CT

The non-contrast exam is acquired at 5 mm intervals with images reconstructed at 2.5 mm.

Non-contrast CT images are used to detect diffuse hepatic disease caused by storage and metabolic disorders, such as fatty infiltration or hemochromatosis. Normal liver parenchyma is homogenous and measures between 55 and 65 Hounsfield units (HU), or 10 HU greater than the spleen on non-contrast images. Hepatic fatty infiltration lowers the HU and is diagnosed when the spleen measures ten or more HU than the liver (Fig. 1.1).

The abnormal hepatic accumulation of copper, glycogen, or iron elevates the hepatic HU to values above 65 HU [1].

Non-contrast CT images provide baseline Hounsfield units for comparison with contrast-enhanced images to evaluate for lesion enhancement and distinguish this enhancement from hemorrhage or calcifications. Non-contrast images are also used to evaluate Lipiodol distribution after intra-arterial embolization of hepatic tumors.

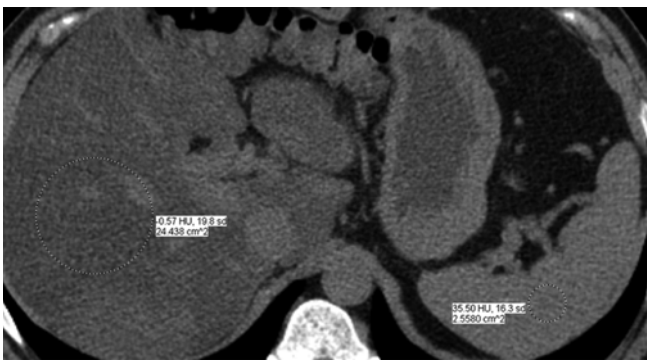

Fig. 1.1 Axial non-contrast CT image shows that the liver measures 10 HU less than the spleen secondary to fatty infiltration

Contrast-Enhanced CT

A liver protocol is used to evaluate most hepatic pathology, improving hepatic lesion identification and characterization [2, 3]. The protocol consists of non-contrast phase followed by multiphasic dynamic imaging with an intravenous iodinated contrast agent. A 16-detector scanner or greater needs to be used so that the entire liver can be covered during the late arterial phase. Multidetector scanners also allow the liver to be imaged at low energy or 80 kVp. An iodinated contrast material has a higher attenuation on 80 kVp images compared to high-energy or 140 kVp images, and low-kVp images can improve hepatic lesion detection [4]. Unfortunately in larger patients, a low kVp can produce images with too much noise to be diagnostic. We use automated exposure control (AEC) to adapt the tube current to the patient's size to obtain quality images. AECs also lower radiation dose and have been shown to reduce the mean tube current by 20–68 % compared to exams that are obtained at constant tube current [5].

T. Sagebiel, MD (✉) • J. Szkarluk, MD, PhD
Department of Diagnostic Radiology, The University of Texas MD Anderson Cancer Center, Houston, TX, USA
e-mail: Tsagebiel@mdanderson.org; jszklaru@mdanderson.org

K.M. Elsayes (ed.), *Cross-Sectional Imaging of the Abdomen and Pelvis: A Practical Algorithmic Approach*,
DOI 10.1007/978-1-4939-1884-3_1, © Springer Science+Business Media New York 2015

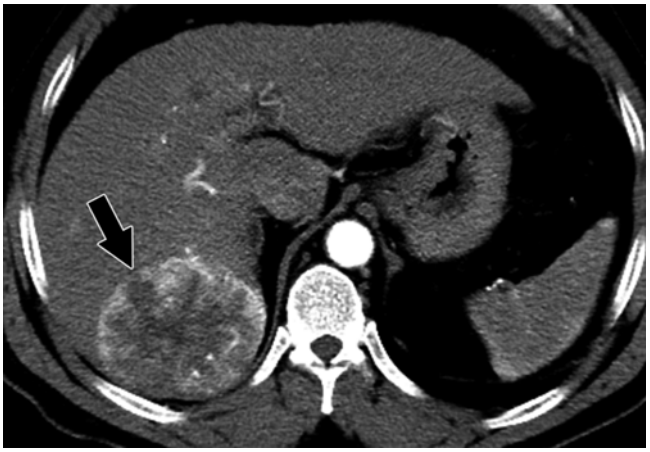

Fig. 1.2 Axial contrast-enhanced CT shows the early enhancement of the hypervascular HCC (*black arrow*) during the arterial phase

Fig. 1.3 Axial contrast-enhanced CT shows hypovascular colon cancer metastases (*white arrows*) during the portal venous phase

We also use reconstruction algorithms to enhance image quality of lower-dose scans.

At our institution, the images are obtained at 5 mm and reconstructed into 2.5 mm images.

Intravenous contrast should be administered using bolus tracking to ensure that accurate hepatic perfusional phases are obtained, regardless of a patient's cardiac function, blood volume, or visceral perfusion. Bolus tracking monitors a target vessel or organ's attenuation and begins the exam when the region of interest (ROI) reaches a designated threshold. Our institution places the ROI in the abdominal aorta near the celiac axis.

The late arterial phase is the first phase and is the most difficult phase to capture. Our liver protocol images the late arterial phase 17 s after the ROI reaches 100 HU, or approximately 30–35 s after the intravenous contrast was administered at a rate of 4–6 cc/s.

The late arterial phase is useful for identifying hypervascular lesions, including hepatocellular cancer (HCC), melanoma, and neuroendocrine metastases. The hepatic arterial anatomy can also be evaluated during this phase (Fig. 1.2).

The portal venous phase is the second phase and is acquired approximately 60 s after contrast administration. The portal venous phase is used to identify hypovascular metastases such as those from colon cancer (Fig. 1.3). This phase is also used to evaluate the portal venous system and to determine segmental anatomy.

The excretory phase is the final phase and is acquired 3–5 min after contrast administration. This phase allows for additional characterization of lesions identified in the previous two phases. For example, a hypervascular lesion in a cirrhotic liver that has contrast washout on this phase is suspicious for HCC, while a lesion with progressive, centripetal filling is consistent with a hemangioma.

Hepatic lesions that retain contrast, such as confluent hepatic fibrosis, cholangiocarcinomas, and giant hemangiomas, may need a 10 min delayed phase for additional evaluation [6, 7].

Magnetic Resonance Imaging

Magnetic resonance imaging (MRI) is increasingly utilized as the first-line modality for hepatic imaging. MRI's prior limitations, which included long exam times and images with low temporal and spatial resolution and poor signal-to-noise ratios, have been improved with new advanced imaging techniques. The clear advantages MRI has over computed tomography (CT), which is currently the most common modality used for hepatic imaging, are MRI's superb tissue contrast and lack of ionizing radiation. The recent introduction of hepatobiliary contrast agents has created new potential applications for MRI hepatic evaluation. The following sections will review the commonly used sequences for hepatic imaging. For these sequences, the normal liver signal relative to adjacent organs and the relative signal of the liver to common focal liver lesions and diffuse pathologies will also be presented.

Hepatic imaging is best performed at 1.5 or 3 T strength magnets using a multichannel phased-array coil. The basic MRI protocol for hepatic imaging has matured to include four sequences:

- Axial T1-weighted imaging (T1WI)
- Axial T2-weighted imaging (T2WI)
- Axial diffusion-weighted imaging (DWI)
- Axial precontrast and postcontrast imaging

T1-Weighted Imaging

T1-weighted imaging (T1WI) evaluation of the liver uses spoiled gradient echo (SPGR) techniques (GE Medical Systems, Milwaukee, USA) *GE nomenclature will be used throughout. Please refer to* Table 1.1, Appendix A. SPGR sequences can be obtained during a single breath hold, which minimizes respiratory motion artifact. Parallel imaging permits the acquisition of both in-phase (IP) and opposed-phase

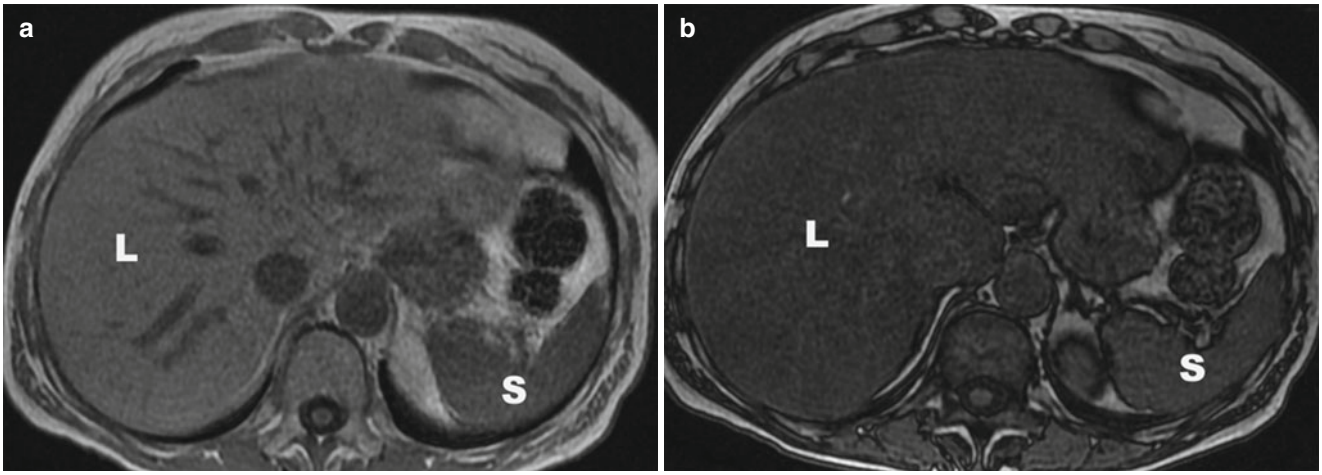

Fig. 1.4 (**a**) Axial in-phase image shows that the liver (*L*) signal is higher than the spleen (*S*) signal. (**b**) Axial out-of-phase image shows that the liver signal has dropped relative to the spleen secondary to fatty infiltration. *L* liver, *S* spleen

(OP) images during a single breath hold, when using 5 mm slice thickness or 30 slices, eliminating registration errors [8]. Parallel imaging is able to speed up scan time because only a portion of the k-space data is sampled with an array of receiver coils. The undersampled data can then be reconstructed into images using various algorithms [9]. In a 1.5T scanner, OP images are usually acquired at a TE of 2.1 ms while IP images are acquired at a TE of 4.2 ms.

The terms in-phase and out-of-phase refer to the relative phases of the signal of water and fat protons. In the out-of-phase series, the fat signal will cancel with corresponding water signal. In contrast, the in-phase series will result in the addition of both proton signals.

The normal liver will have the same signal intensity on IP T1WI and OP T1WI. The liver is slightly hyperintense to the spleen, muscle, and kidneys. The signal is dependent on the liver's fat and iron content. In the setting of fatty infiltration, the liver signal increases on IP T1WI and decreases on OP T1WI (Fig. 1.4). This is also useful to detect microscopic fat within lesions. In the setting of iron overload in the liver, the liver is brighter on the OP relative to the IP images. This is due to the T2*-related signal loss on the longer echo time [10]. Similar susceptibility effects from iron and other metals can be identified with IP and OP imaging. Susceptibility artifacts occur at interfaces of substances with different magnetic susceptibilities. Magnetic susceptibility artifacts are also commonly seen at interfaces between air and tissue, such as in the bowel. These artifacts are more pronounced on IP images secondary to the longer echo time [11]. Spin echo (SE)-based techniques can be used to decrease susceptibility artifacts, but these SE series are very long.

In addition to fat, protein and blood are bright on IP T1WI, and IP T1WI may be useful in identifying posttraumatic hematomas and hemorrhagic malignancies [6]. Melanin, copper, and glycogen are also bright on IP T1WI. Lesions that are hypointense to the normal liver on IP T1WI include metastases, cysts, hemangiomas, and areas of fibrosis. Finally, IP T1WI is not fat saturated and provides excellent definition of the various fat planes in the evaluation of hepatic anatomy.

T2-Weighted Imaging

There are a variety of techniques that can be used to obtain T2-weighted imaging (T2WI) of the liver. The most commonly used is fast spin-echo (FSE) technique. A variant of FSE are FRFSE and SSFSE (GEMS) sequences. Another T2WI imaging technique is diffusion-weighted imaging. In this section we review the imaging parameters for these various series.

FSE

Fast spin-echo (FSE) sequences significantly shorten T2WI scan times by using a train of echoes to fill multiple lines of K-space per TR (echo train length) (ETL) [12, 13]. The ETL varies but it is commonly between 16 and 21. The length of the ETL will affect the signal-to-noise *ratio* (SNR) and contrast-to-noise ratio (CNR). FSE image contrast is also reduced secondary to j-coupling interactions which cause fat to have a bright signal on FSE images rather than the dark-to-intermediate signal fat has on traditional SE images [14]. A reduction of SNR and CNR can make the detection of liver lesions more difficult [15]. T2WI is commonly obtained with an echo time (TE) of 60–80 ms. A longer TE will result in increased contrast with overall signal loss. The TR of FSE is over 4s. Fat suppression can be used to improve

image contrast and hepatic lesion detection. The FSE technique decreases artifacts. T2WI can be obtained with respiratory-triggered techniques or variants of navigator (GEMS)/propeller techniques. These latter techniques reduce the motion artifact due to breathing or pulsation.

On T2WI, the normal liver signal is usually hypointense to the spleen, kidneys, and pancreas. Most hepatic pathology, such as metastatic disease and hepatocellular carcinoma, are hyperintense to the normal hepatic parenchyma. Water-like consistencies have a high T2 signal, so T2-weighted sequences are also useful for detecting cysts and hemangiomas and for evaluating the biliary system. A fatty liver will result in some signal loss if the T2WI is obtained with fat saturation. A dramatic loss of the liver signal is seen in the setting of iron deposition. This is best evaluated when compared to the muscle, as the pancreas and spleen may also have iron overload in the setting of primary hemochromatosis [6, 10].

SSFSE

Single-shot fast spin-echo (SSFSE) sequences (GEMS) are an extreme version of the multi-echo spin technique, where a single excitation pulse precedes all the echoes obtained in a single acquisition. The ETL is very long (>60). As k-space is symmetric, SSFSE acquires enough echoes to fill a little more than half of the k-space (0.6NEX). In the setting of a matrix of 128 phase-encoding steps, this corresponds to an ETL of 77 echoes. The needed data to fill the center of k-space can be obtained within a fraction of a second. Compared to FSE, SSFSE images have less motion-related artifact secondary to the faster acquisition time, but SSFSE images have more blurring from the long ETL [16]. SSFSE sequences also have inherently poorer SNR and T2 contrast secondary to the long radiofrequency pulse train and cannot be used to evaluate for solid tumors [17]. SSFSE sequences are commonly used to obtain a quick T2 survey of the abdomen that can also be used as the localizer for the remainder of the exam.

FRFSE

To achieve breath-hold T2WI, fast relaxation fast spin-echo (FRFSE, GEMS) sequences are another option. FRFSE adds a negative 90° pulse to the end of the echo train used in FSE sequences. This additional pulse aligns protons in tissues with long T2 values into the longitudinal plane from the transverse plane, allowing much faster recovery of these tissues while improving the contrast between tissues with long and short T2. The TE values for FRFSE are similar to FSE techniques (60–80 ms). The TR for FRFSE is 2S per ETL. This relative short TR allows breath-hold technique (slices – 50 slices at 5 mm) [14]. FRFSE images can be used to detect solid lesions (Fig. 1.5).

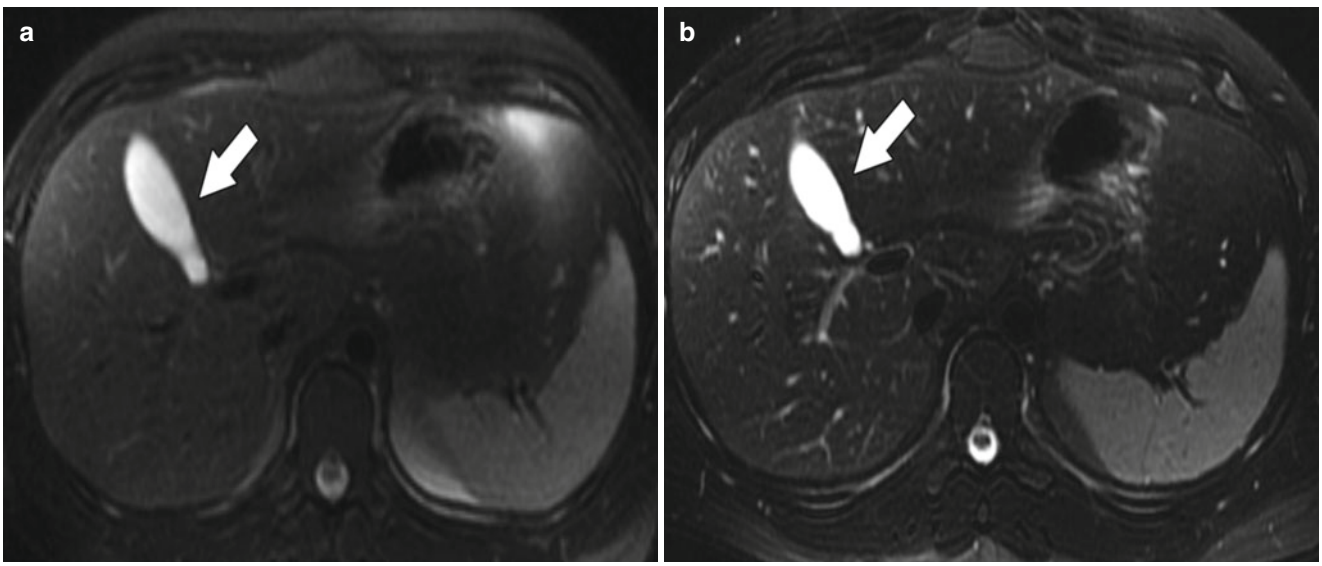

Fig. 1.5 (**a**) Axial T2 fat-suppressed FSE image shows the high signal in the fluid-filled gallbladder (*arrow*). (**b**) Axial T2 fat-suppressed FRFSE image from the same study again shows the high signal gallbladder (*arrow*), but notice the improved visualization of the biliary radicles secondary to the improved T2 contrast

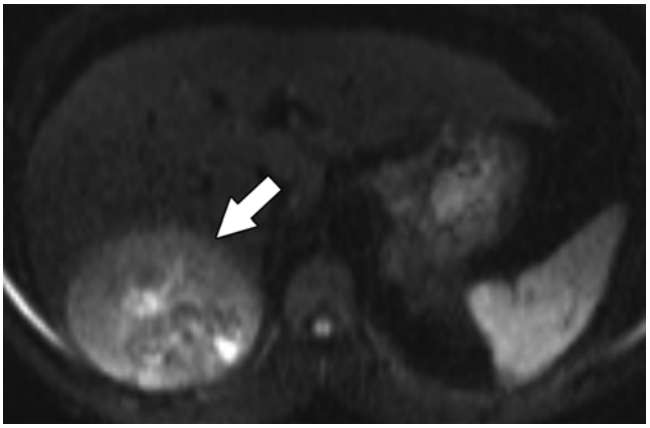

Fig. 1.6 Axial DWI image shows the high signal from restricted diffusion in an HCC (*white arrow*)

Diffusion-Weighted Imaging

Diffusion-weighted imaging (DWI) is also a variant of T2WI. The images are obtained with echo planar imaging (EPI), using breath-hold, free-breathing, or respiratory-triggered techniques. Respiratory-triggered EPI is recommended over breath-hold EPI because its multiple acquisition technique produces images with a better SNR and allows for the use of more *b* values [18]. It is best to obtain diffusion gradients in three orthogonal planes to produce a stronger gradient with shorter TEs and less susceptibility, but adequate images can be obtained with only one axis (*z*-axis) gradient [19].

DWI uses two or more identical diffusion-sensitizing gradient pulses separated by a 180° refocusing pulse to change the phase of normal, unrestricted water protons so that they lose signal while abnormal, restricted water protons retain their phase and signal. The amount of signal loss is inversely related to the degree of water proton motion or apparent diffusion coefficient (ADC) and the *b* value. The *b* value is the sum of the diffusion-weighted gradient amplitude, applied gradient duration, and the time interval between the applied gradients or gradient separation.

Changing the *b* value can alter diffusion sensitivity and typical *b* value range from 400 to 800 s/mm^2. The larger the *b* value, the more the image signal is based on diffusion properties, while smaller *b* values will have more signal contribution from T2 effects. The *b* values used for hepatic lesion detection should be less than 100 s/mm^2. This low *b* value creates images with high tissue contrast that aides in lesion detection. Higher *b* values, 500 s/mm^2 or greater, provide more information about a lesion's diffusion properties and are used for lesion characterization.

DWI technique has been reported to be used to:

1. Improve detection of small tumors secondary to greater lesion conspicuity
2. Assess tumor response to various treatments [18]

Most solid lesions usually have restricted diffusion or high signal on DWI sequences (Fig. 1.6) and low signal on the ADC map. The reader must be aware of T2 shine-through effect, which can be seen in lesions that are normally bright on T2-weighted images, such as cysts, but they are not areas of restricted diffusion. There is a reduction in signal intensity but it is not apparent on visual inspection of the image. ADC maps are created to remove the T2 shine-through artifacts with resultant images providing pure diffusion information. True water proton restriction will have a high signal on diffusion-weighted images and a low signal on the ADC map, while T2 shine-through effect will be bright on both [20]. The normal liver will have a lower signal than the spleen, liver, and kidneys on DWI. The liver signal will increase with increasing *b* values.

FIESTA

Fast imaging employing steady-state acquisition (FIESTA, GEMS; Appendix A) is a balanced steady-state free-precession (gradient echo) sequence that uses ultrashort TR and TE values to acquire images quickly. FIESTA produces high-resolution images with better image contrast and signal-to-noise compared to SSFSE sequences [21]. FIESTA images have mixed image weightings, and the image contrast is determined by the T2/T1 ratio. FIESTA sequences are insensitive to motion artifacts. FIESTA sequence offers excellent visualization of the vascular anatomy secondary to its fluid sensitivity and insensitivity to flow void artifacts, which may be useful to evaluate the hepatic and portal veins in patients who cannot receive contrast (Fig. 1.7) [6]. This sequence can also be used to evaluate the vasculature for surgical planning. FIESTA sequences are prone to susceptibility artifact, which can be reduced by keeping the TR short (TR = 4.0 ms; TE = 1; flip angle = 75). The normal liver signal will be lower than the spleen, kidneys, and pancreas on FIESTA images, since the images are usually more heavily T2 weighted than T1 weighted. Fat-containing lesions such as adenomas are hypointense to the normal liver parenchyma on FIESTA images. Fluid-containing structures such as cysts and hemangiomas will be hyperintense.

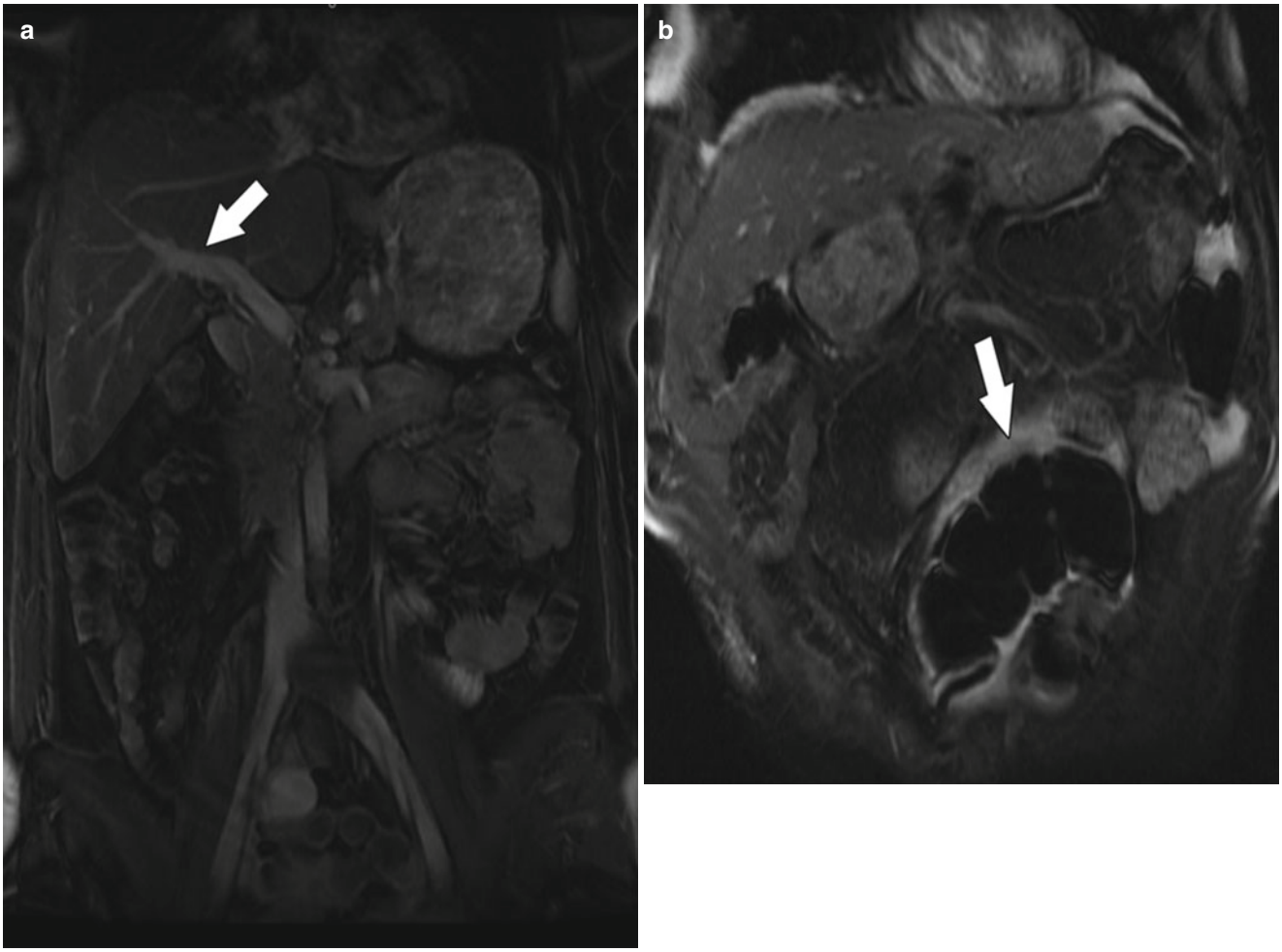

Fig. 1.7 (**a**) Coronal FIESTA image shows an excellent visualization of the vasculature, including the portal vein (*white arrow*). (**b**) Coronal FIESTA image shows the prominent susceptibility artifact from bowel gas (*white arrow*) which is a disadvantage of this sequence

Contrast-Enhanced Hepatic MR Imaging

Dynamic contrast-enhanced (DCE) MRI of the liver is used for lesion detection and for lesion characterization, since certain types of dynamic enhancement patterns are seen with particular disease processes and can narrow the differential diagnosis.

Arterial phase images are generally the most important, but timing the late arterial phase is technically challenging. One suboptimal method is to use a standard delay, such as 20 s, following the administration of contrast. This method does not compensate for cardiac output or other physiologic delays and results are variable. Acquiring multiple consecutive arterial phases following contrast administration is another technique. This maximizes the chance to accurately capture the arterial phase but requires a decrease in phase-encoding steps to shorten the scan time within a breath hold. Fluoro-triggered acquisitions initiate scanning after short delay once contrast is visualized in the aorta or at the level of the pulmonary arteries. The optimum timing delay used in these methods depends on the k-space filling method of the MR software. Dynamic imaging has recently been benefitted from the introduction of MRI techniques that use the temporal or spatiotemporal redundancy of k-space data to shorten scan times and to produce images with higher spatial and temporal resolution. Only a fraction of the redundant k-space information needs to be captured, or "undersampled," while the rest of the data can be recovered by using models that predict patterns of data redundancy. The "keyhole" technique is one of the acceleration techniques [22]. Keyhole takes advantage of the fact that most of the MR image contrast and signal is derived from data at the center of the k-space and updates this data frequently while sampling data from the periphery of the k-space only once or twice. Acceleration techniques are limited by the fidelity of the model used for data reconstruction, and any errors in the model will be transferred to the final images. Increasing the frequency of data sampling along a time axis improves the images fidelity but at the expense of the scan length [23].

In addition to the late arterial phase, images are also acquired during the portal venous (60 s) and excretory phases (120–180 s).

The contrast agents routinely used in MR imaging can be divided into two groups. The first group contains the nonspecific, extracellular agents, which are the oldest and most widely used MR contrast agents. Nonspecific agents rely on a lesion's inherent vascularity and enhancement dynamics for detection and characterization [24].

When extracellular agents are used to characterize lesions by their enhancement pattern, it is crucial that images are acquired at the right time, since enhancement may be transient.

Gadolinium chelates make up the nonspecific group and include Gd-DTPA (Magnevist, Bayer Schering AG) and Gd-DTPA-BMA (Omniscan, GE Healthcare). Gadolinium is an extracellular paramagnetic agent that shortens tissue T1 relaxation times and increases their signal intensity on T1-weighted images. Its redistribution from intravascular to extracellular spaces is quick, and it is usually injected at a dose of 0.1–0.2 mmol/kg of the patient's weight and at a rate of 2 cc/s.

Gadolinium agents are excreted by the renal system and have been associated with nephrogenic systemic fibrosis in patients with impaired renal function and are not recommended for use in patients with a glomerular filtration rate (GFR) of less than 30 cc/min/1.73 m^2 [25].

Fat suppression should be used for postcontrast imaging to improve the contrast and visualization of enhancing lesions. Hypervascular metastases are better detected on the late arterial phase, while hypovascular metastases are better detected on the portal venous phase.

Precontrast images should be obtained so materials that have a high T1 signal such as blood or melanin are not mistaken for enhancement.

Gd-EOB-DTPA

Gadolinium ethoxybenzyl dimeglumine (Gd-EOB-DTPA – known as Eovist, Primovist, and EOB-Primovist – Bayer Pharmaceuticals) is a gadolinium-based hepatobiliary-specific agent that is actively transported into hepatocytes and partially eliminated through the biliary system, making it useful for evaluating the liver and biliary tree. Currently, Gd-EOB-DTPA has been used for detecting hepatocellular carcinomas (HCC), detecting liver metastases in potentially operable patients, and characterization of FNH. MRI using Gd-EOB-DTPA has been shown to be superior to MDCT in the detection of HCCs smaller than 1 cm [26]. Gd-EOB-DTPA has also been used to evaluate the biliary tree for strictures, bile leaks, and preoperative anatomy variants [27].

Gd-EOB-DTPA initially is distributed in the vascular and extravascular spaces and can be used to dynamically image the liver similar to its nonspecific gadolinium counterparts [28]. Next, Gd-EOB-DTPA is taken up by hepatocytes via the OATP1B1 and B3 transporter polypeptides and excreted into the biliary system by the MRP2 protein during the hepatobiliary phase. Imaging of this hepatobiliary phase should be performed 20 min after contrast administration (REF). As the last phase of contrast administration is obtained at 5 min delay, this leaves a 15 min gap to reach the hepatocyte phase. This time can be used to obtain the DWI and T2WI sequences. The liver is hyperintense to the spleen, pancreas, and kidneys during the hepatocyte phase. Gd-EOB-DTPA will accumulate in lesions with hepatocytes, such as focal nodular hyperplasia. Metastases and most hepatocellular carcinomas which have no or few functioning hepatocytes will not accumulate Gd-EOB-DTPA and will appear as low-signal lesions within the liver (Fig. 1.8). Unfortunately, hepatocellular carcinomas can

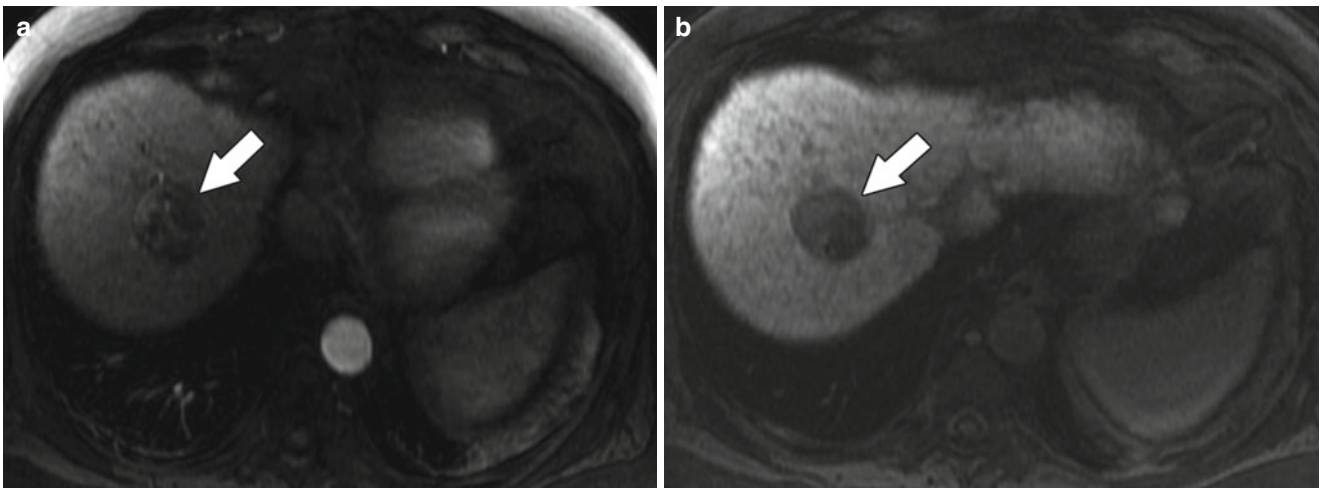

Fig. 1.8 (**a**) Axial contrast-enhanced MRI using Gd-EOB-DTPA shows enhancement of an HCC (*white arrow*) during the arterial phase. (**b**) The hepatobiliary phase shows the lack of Gd-EOB-DTPA in the HCC (*white arrow*)

potentially accumulate Gd-EOB- DTPA [29]. Approximately 50 % of Gd-EOB-DTPA is excreted into the bile, and the remainder is excreted by the kidneys [26]. The percentage of Gd-EOB-DTPA excreted by the kidneys will increase in patients with hepatic dysfunction and vice versa [30]. Patients with bilirubin values greater than 3 g/dl should not be imaged with Gd-EOB-DTPA, given the high likelihood of a nondiagnostic exam. Gd-EOB-DTPA has a higher T1 relaxivity compared to Gd-DTPA and only requires a dose of 0.025 mmol/kg. There are some potential problems related to this low dosage. The small volume of contrast used can cause problems in correctly timing the image acquisition [31]. Doubling the Gd-EOB-DTPA dosage has been suggested as a solution to these problems, but the clinical impact of the increased dosage is unknown. No cases of nephrogenic systemic fibrosis have been linked with Gd-EOB-DTPA. The uptake of Gd-EOB-DTPA by hepatocytes has been proposed to evaluate diffuse liver disease. It has been reported that in the setting of liver cirrhosis and fibrosis, there is a delay in the uptake of Gd-EOB-DTPA. This patient population requires a longer delay in the hepatocyte phase (>40 min) [32].

Gd-BOPTA

Gadobenate dimeglumine (Gd-BOPTA, MultiHance, Bracco Imaging) is an older hepatocyte-specific agent. Like Gd-EOB-DTPA it increases the contrast between the normal liver parenchyma and HCC and metastases on the hepatobiliary phase, making their detection easier [33]. Gd-BOPTA differs from Gd-EOB-DTPA in that its hepatobiliary excretion is only 5 %. It also has a lower T1 relaxivity than Gd-EOB-DTPA. Gd-BOPTA in the hepatocyte phase requires scanning to be delayed 60–120 min after injection. The recommended dose is 0.05 mmol/kg [26].

Conclusion

Thanks to emerging technology and sequences, MRI is now a valid modality for first-line hepatic imaging. Hepatic MRI exams can be performed in a reasonable time frame (15–20 min scan time). MRI's role in evaluating oncologic patients has also been expanded by the arrival of hepatobiliary agents, which add specificity to hepatic lesion diagnoses and improve lesion detection in potential surgery patients.

Appendix A

Table 1.1 MRI sequence vendor specific nomenclature

Sequence type	GE name	Siemens name	Phillips name	Hitachi name	Toshiba name
Spoiled gradient echo	SPGR	FLASH	T1-FFE	RF Spoiled SARGE, RSSG	FastFE
Spin echo	SE	SE	SE	SE	SE
Fast spin echo	FSE	TSE	TSE	FSE	FSE
Ultrafast spin echo	SSFSE	HASTE	SSTSE	SSFSE	FASE
Fast recovery fast spin echo	FRFSE	RESTORE	DRIVE	Driven Equilibrium FSE	T2 Puls FSE
Diffusion-weighted imaging	DWI	DWI	DWI	DWI	DWI
Balanced gradient echo	FIESTA	TrueFISP	Balanced FFE	Balanced SARGE, BASG	True SSFP
Echo planar imaging	EPI	EPI	EPI	EPI	EPI
3D volume ultrafast gradient echo	Fast SPGR LAVA	TurboFLASH VIBE	T1-TFE THRIVE	TIGRE	Fast FE QUICK 3D

References

1. Dwyer A, et al. Influence of glycogen on liver density: computed tomography from a metabolic perspective. J Comput Assist Tomogr. 1983;7(1):70–3.
2. Kamel IR, Liapi E, Fishman EK. Multidetector CT of hepatocellular carcinoma. Best Pract Res Clin Gastroenterol. 2005;19(1):63–89.
3. Monzawa S, et al. Dynamic CT for detecting small hepatocellular carcinoma: usefulness of delayed phase imaging. AJR Am J Roentgenol. 2007;188(1):147–53.
4. Yeh BM, et al. Dual-energy and low-kVp CT in the abdomen. AJR Am J Roentgenol. 2009;193(1):47–54.
5. Mulkens TH. Dose management in Multidetector Computed Tomography (MDCT): modalities for dose reduction and clinical studies. Belgium: Universiteit Antwerpen; 2008. 223.
6. Boll DT, Merkle EM. Diffuse liver disease: strategies for hepatic CT and MR imaging. Radiographics. 2009;29(6):1591–614.
7. Goshima S, et al. MDCT of the liver and hypervascular hepatocellular carcinomas: optimizing scan delays for bolus-tracking techniques of hepatic arterial and portal venous phases. AJR Am J Roentgenol. 2006;187(1):W25–32.
8. Yu JS, et al. Hepatic MRI using the double-echo chemical shift phase-selective gradient-echo technique. AJR Am J Roentgenol. 2007;188(1):W49–56.
9. Deshmane A, et al. Parallel MR imaging. J Magn Reson Imaging. 2012;36(1):55–72.
10. Alustiza JM, Castiella A. Liver fat and iron at in-phase and opposed-phase MR imaging. Radiology. 2008;246(2):641.
11. Westbrook C, Roth CK, Talbot J. MRI in practice. 3rd ed. Malden: Blackwell; 2005. xii, 410 p.
12. Low RN. Abdominal MRI, advances in the detection of liver tumours and characterisation. Lancet Oncol. 2007;8(6):525–35.
13. Li T, Mirowitz SA. Fast T2-weighted MR imaging: impact of variation in pulse sequence parameters on image quality and artifacts. Magn Reson Imaging. 2003;21(7):745–53.
14. Huang J, et al. Utility of breath-hold fast-recovery fast spin-echo t2 versus respiratory-triggered fast spin-echo T2 in clinical hepatic imaging. AJR Am J Roentgenol. 2005;184(3):842–6.
15. Semelka RC. Abdominal-pelvic MRI. Hoboken: Wiley; 2006.
16. Leyendecker JR, Brown JJ, Merkle EM. Practical guide to abdominal & pelvic MRI. 2nd ed. Philadelphia: Wolters Kluwer Health/ Lippincott Williams & Wilkins; 2011. ix, 406 p.
17. Morrin MM, Rofsky NM. Techniques for liver MR imaging. Magn Reson Imaging Clin N Am. 2001;9(4):675–96. v.
18. Taouli B, Koh DM. Diffusion-weighted MR imaging of the liver. Radiology. 2010;254(1):47–66.
19. Low RN, Gurney J. Diffusion-weighted MRI (DWI) in the oncology patient: value of breathhold DWI compared to unenhanced and gadolinium-enhanced MRI. J Magn Reson Imaging. 2007;25(4):848–58.
20. Chandarana H, Taouli B. Diffusion-weighted MRI and liver metastases. Magn Reson Imaging Clin N Am. 2010;18(3):451–64. x.
21. Bhosale P, Ma J, Choi H. Utility of the FIESTA pulse sequence in body oncologic imaging: review. AJR Am J Roentgenol. 2009;192(6 Suppl):S83–93. Quiz S94–7.
22. Motosugi U, et al. Delay before the hepatocyte phase of Gd-EOB-DTPA-enhanced MR imaging: is it possible to shorten the examination time? Eur Radiol. 2009;19(11):2623–9.
23. Tsao J, Kozerke S. MRI temporal acceleration techniques. J Magn Reson Imaging. 2012;36(3):543–60.
24. Yoon SH, et al. Multiphasic MDCT enhancement pattern of hepatocellular carcinoma smaller than 3 cm in diameter: tumor size and cellular differentiation. AJR Am J Roentgenol. 2009;193(6):W482–9.
25. Sadowski EA, et al. Nephrogenic systemic fibrosis: risk factors and incidence estimation. Radiology. 2007;243(1):148–57.
26. Reimer P, Schneider G, Schima W. Hepatobiliary contrast agents for contrast-enhanced MRI of the liver: properties, clinical development and applications. Eur Radiol. 2004;14(4):559–78.
27. Karabulut N, Cakmak V, Kiter G. Confident diagnosis of bronchobiliary fistula using contrast-enhanced magnetic resonance cholangiography. Korean J Radiol. 2010;11(4):493–6.
28. Van Beers BE, Pastor CM, Hussain HK. Primovist, Eovist: what to expect? J Hepatol. 2012;57(2):421–9.
29. Husarik DB, et al. Contrast enhanced liver MRI in patients with primary sclerosing cholangitis: inverse appearance of focal confluent fibrosis on delayed phase MR images with hepatocyte specific versus extracellular gadolinium based contrast agents. Acad Radiol. 2011;18(12):1549–54.
30. Gschwend S, et al. Pharmacokinetics and imaging properties of Gd-EOB-DTPA in patients with hepatic and renal impairment. Invest Radiol. 2011;46(9):556–66.
31. Tamada T, et al. Dynamic contrast-enhanced magnetic resonance imaging of abdominal solid organ and major vessel: comparison of enhancement effect between Gd-EOB-DTPA and Gd-DTPA. J Magn Reson Imaging. 2009;29(3):636–40.
32. Tamada T, et al. Gd-EOB-DTPA-enhanced MR imaging: evaluation of hepatic enhancement effects in normal and cirrhotic livers. Eur J Radiol. 2011;80(3):e311–6.
33. Petersein J, et al. Focal liver lesions: evaluation of the efficacy of gadobenate dimeglumine in MR imaging–a multicenter phase III clinical study. Radiology. 2000;215(3):727–36.

Diagnostic Approach of Focal and Diffuse Hepatic Diseases

2

Ehab Youssef, Richard L. Baron, and Khaled M. Elsayes

Anatomical Background

The liver is the largest organ in the human body reaching up to 1500 g in adults. Previously, the liver was anatomically divided into the right lobe (which is further subdivided into anterior and posterior segments) and left lobe (which is further subdivided into medial and lateral segments). The current classification system of liver segmental anatomy (Couinaud and Bismuth systems) divides the liver into eight segments, and each segment is an independent functioning unit, which has its own vascular pedicle (arterial, portal venous, and lymphatic) and biliary drainage. This has fueled technical progress in liver surgery and transplantation. The intrahepatic vasculature is clearly seen with enhanced CT and MRI, which makes these modalities ideally suited to the study of the functional segmental anatomy of the liver (Fig. 2.1) [1].

There are three fissures that help define hepatic lobes and the major hepatic segments. The interlobar fissure (separating the right and left hepatic lobes) is located along the inferior liver margin, oriented along a line passing through the gallbladder fossa inferiorly and the middle hepatic vein superiorly. The interlobar fissure is usually difficult to identify, but it is well defined in some patients. The left intersegmental fissure (fissure for the ligamentum teres) forms a well-defined cleft which is sagittally oriented in the lower left hepatic lobe and divides the left lobe into lateral and medial segments (between segments II/III peripherally and IV centrally). The ligamentum teres, which represents obliterated left umbilical vein, normally contains small amount of fat, runs through this fissure after entering it via the free margin of the falciform ligament. The third fissure – fissure for ligamentum venosum – is oriented in a coronal or oblique plane between the posterior aspect of the left lateral hepatic segment and the anterior aspect of the caudate lobe. This fissure forms a continuum with the intersegmental fissure. The fissure for the ligamentum venosum cuts deeply anterior to the caudate lobe and contains the two layers of the lesser omentum (Fig. 2.2).

This omental reflection forms the porta hepatis where the hepatic artery, portal vein, and hepatic nerve plexus enter the liver and the right and left biliary ducts and lymphatic drainage emerge from it. The caudate lobe is located in the watershed area between the right and left vascular and biliary territory. The caudate lobe drains directly into the IVC and is usually spared in cases of hepatic venous occlusion such as in the Budd–Chiari syndrome [2].

E. Youssef, MD, FRCR
Department of Radiology,
University of Michigan, Ypsilanti, MI, USA
e-mail: ehaby2@gmail.com

R.L. Baron, MD
Department of Radiology,
University of Chicago Medical Center, Chicago, IL, USA
e-mail: rbaron@radiology.bsd.uchicago.edu

K.M. Elsayes, MD (✉)
Department of Diagnostic Radiology, The University
of Texas MD Anderson Cancer Center, Houston, TX, USA
e-mail: kmelsayes@mdanderson.org

K.M. Elsayes (ed.), *Cross-Sectional Imaging of the Abdomen and Pelvis: A Practical Algorithmic Approach*,
DOI 10.1007/978-1-4939-1884-3_2, © Springer Science+Business Media New York 2015

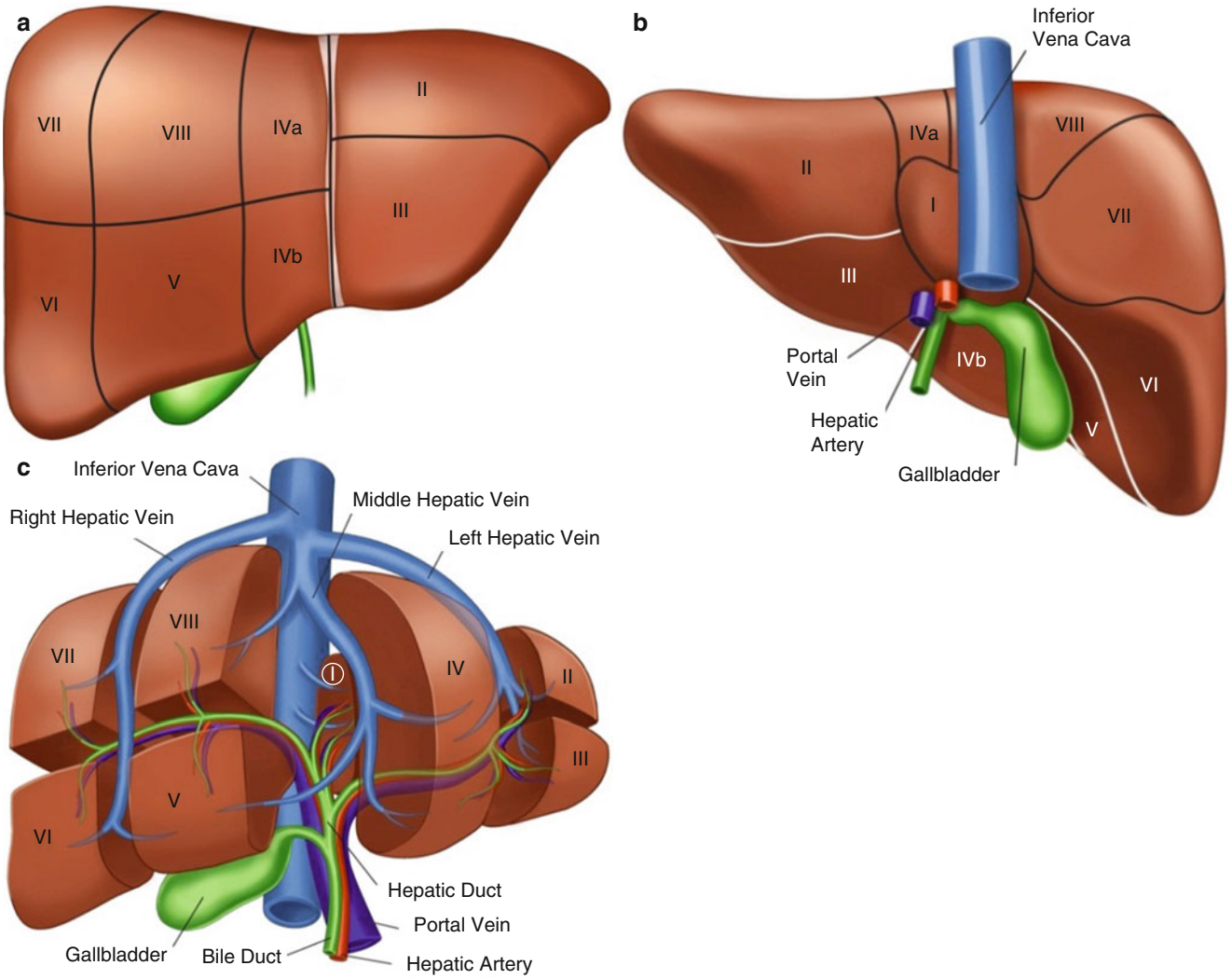

Fig. 2.1 Liver segments in anterior view (**a**), posterior view (**b**), and 3D Illustration (**c**). Segment I: the caudate lobe seen in the posterior view. Segment II: lateral segment of the left hepatic lobe superior to the left portal vein. Segment III: lateral segment of the left hepatic lobe inferior to the left portal vein. Segment IV: medial segment of the left hepatic lobe which is further subdivided by the left portal vein into IVa superiorly and IVb inferiorly. The right portal vein divides the right lobe into segments V/VI inferiorly and segments VII/VIII superiorly. Segments V and VIII are located anteriorly and are demarcated from segments VI and VII posteriorly by the right hepatic vein

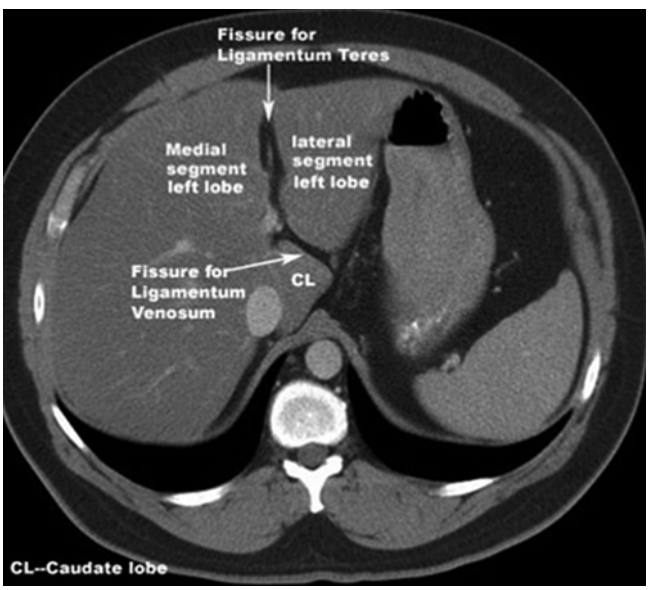

Fig. 2.2 Fissures of the liver; the interlobar fissure (separating right and left hepatic lobes); the left intersegmental fissure (fissure for the ligamentum teres) divides the left lobe into medial and lateral segments. The third fissure is the fissure for ligamentum venosum and is oriented in a coronal or oblique plane between the posterior aspect of the left lateral hepatic segment and the anterior aspect of the caudate lobe. Note that there is a generalized hypodensity of the liver parenchyma in this image secondary to diffuse hepatic steatosis (fatty infiltration)

Table 2.1 Pathological classification of liver diseases

Congenital	Inflammatory
Congenital absence of hepatic segments	Sarcoidosis
Anomalies in position	Primary biliary cirrhosis
Accessory fissures	Diffuse liver disease
Congenital hepatic fibrosis	Fatty liver (steatosis)
Congenital vascular anomaly	Cirrhosis
Congenital focal lesions:	Hemochromatosis
Liver cysts	Wilson disease
Autosomal dominant polycystic kidney disease	Benign focal lesions
Biliary hamartoma	Hemangiomas
Infection	Focal nodular hyperplasia FNH
Hepatitis (viral)	Hepatocellular adenoma
Pyogenic abscess (bacterial)	Adenomas
Amebic abscess	Angiomyolipoma
Hydatid cyst (parasitic)	Malignant focal lesions
Hepatic candidiasis (fungal)	Hepatocellular carcinoma (HCC)
Vascular disorders	Fibrolamellar HCC
Arteriovenous malformation	Cholangiocarcinoma
Budd–Chiari syndrome	Epithelioid hemangioendothelioma
Hepatic infarction	Biliary cystadenoma/cystadenocarcinoma
HELLP syndrome	Angiosarcoma
Peliosis hepatis	Metastasis and hepatic lymphoma
Hepatic artery and portal vein aneurysm	Traumatic, such as:
Portal vein thrombosis	Posttraumatic sequelae
THID/THAD	Posttreatment changes
Portal hypertension	
Hereditary hemorrhagic telangiectasia	

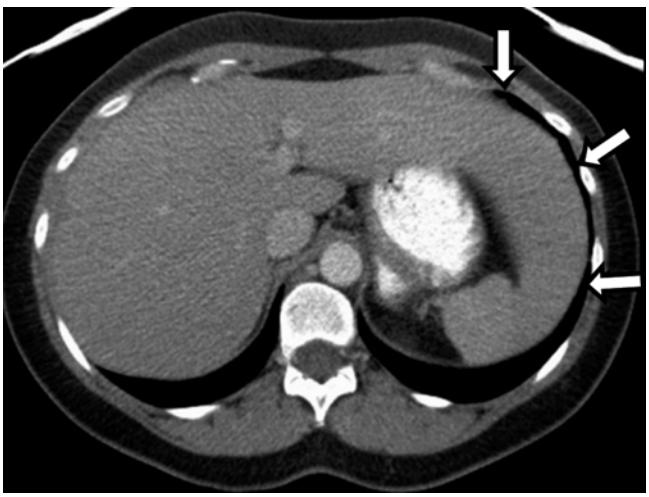

Fig. 2.3 Normal variant of the liver. Axial contrast-enhanced CT image, showing elongated left lobe (*arrows*)

Hepatic disease can be pathologically classified into various categories as illustrated in Table 2.1.

Normal Variants

A spectrum of liver size and shape variations have been reported, including lateral elongation of the lateral segment of the left hepatic lobe (Fig. 2.3), extending to wrap around the spleen, left lobe hypoplasia, and vertical elongation of the right hepatic lobe (Riedel lobe). Familiarity of these normal variants is important, to avoid misdiagnosis of these variants as exophytic mass lesions such as hepatic HCC or adenoma. These variants are more common in females than males [2].

Diaphragmatic insertions can be seen as small wedge-shaped areas, associated with the capsule surface of the liver.

These exhibit low attenuation on CT and demonstrate low signal intensity on T1- and T2-weighted images.

Part One: Algorithmic Diagnostic Approach of Focal Hepatic Lesions

A diagnostic approach should be used to help differentiate various liver lesions based on the spectrum of certain enhancement patterns, imaging features, and attenuation/signal intensity characteristics. Morphologic patterns include solid versus cystic, the presence of calcification, macroscopic fat, and intracellular lipid. Enhancement patterns are seen during specific phases of imaging and include hypoenhancing, arterial enhancing, delayed enhancing, delayed washout and peripheral washout, as well as the presence of a central scar enhancement patterns (Algorithm 2.1). Attenuation characteristics include simple cystic lesions, complex cystic lesions, and calcified lesions as well as lesions containing intracellular lipid, hemorrhagic lesions, and lesions containing macroscopic fat (Algorithm 2.1).

Algorithm 2.1 Algorithmic classification of different patterns of enhancement

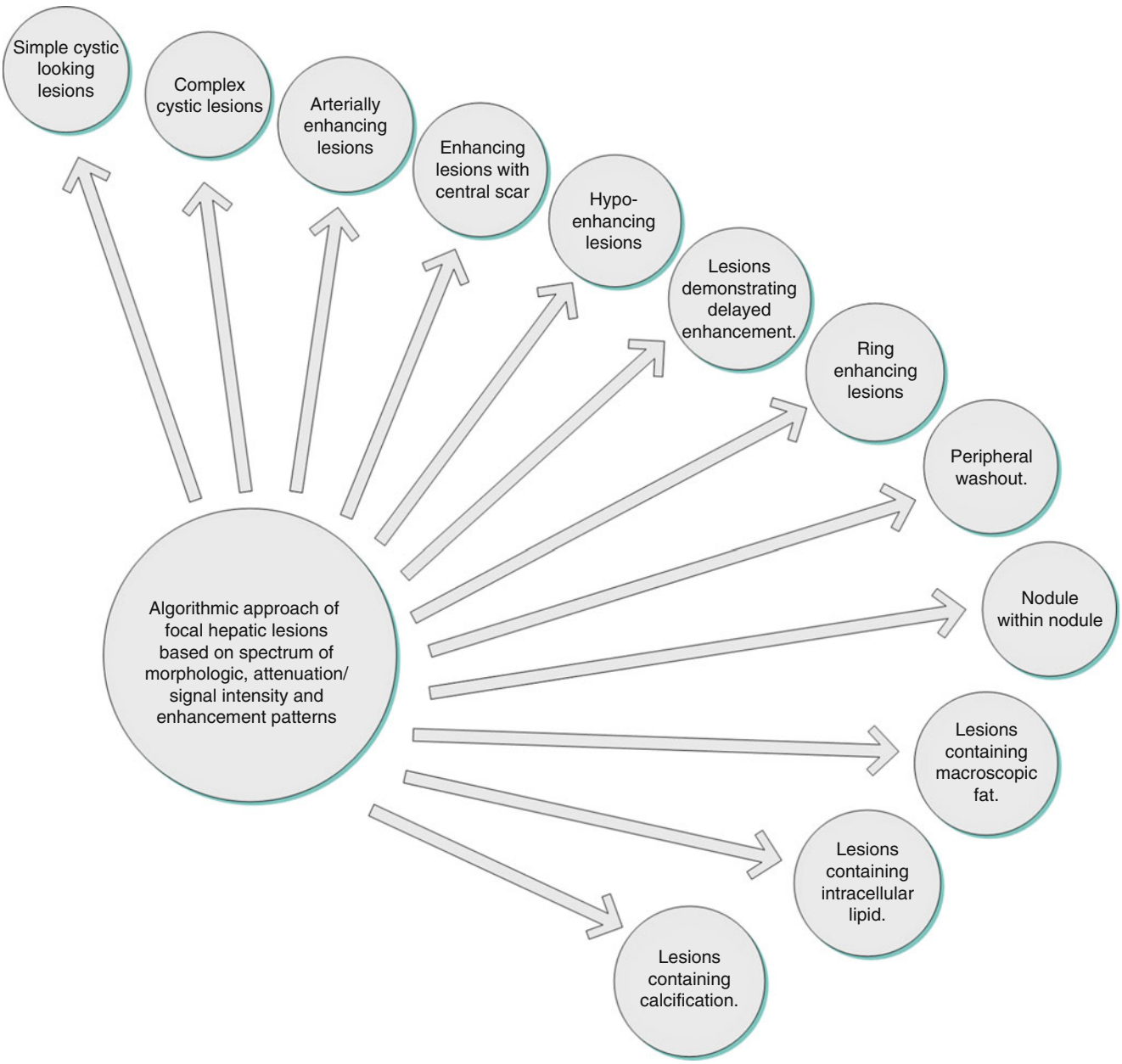

Algorithmic Approach of Focal Hepatic Lesions Based on Spectrum of Morphologic, Attenuation/ Signal Intensity and Enhancement Patterns

Algorithm 2.2 Algorithmic approach of cystic lesions

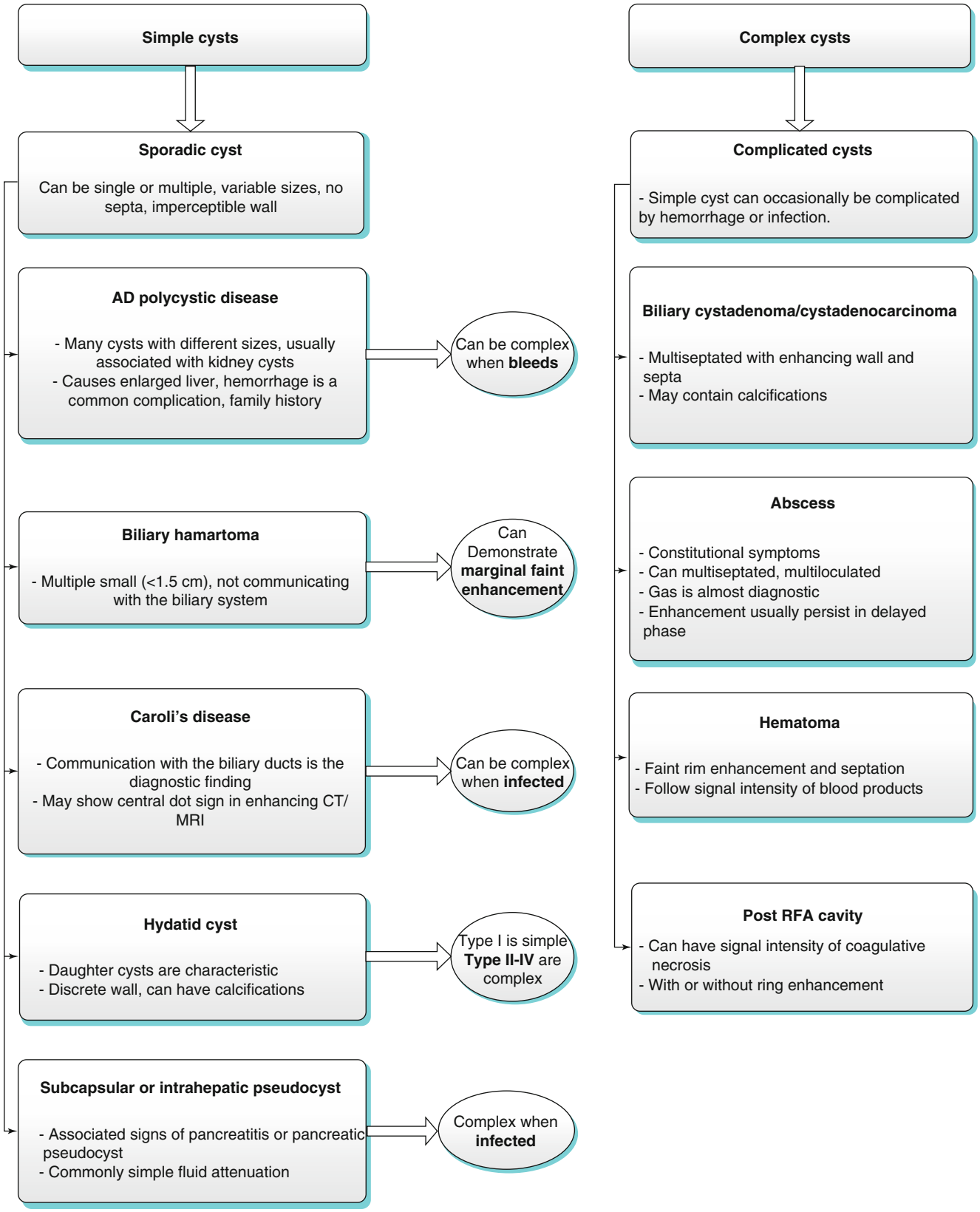

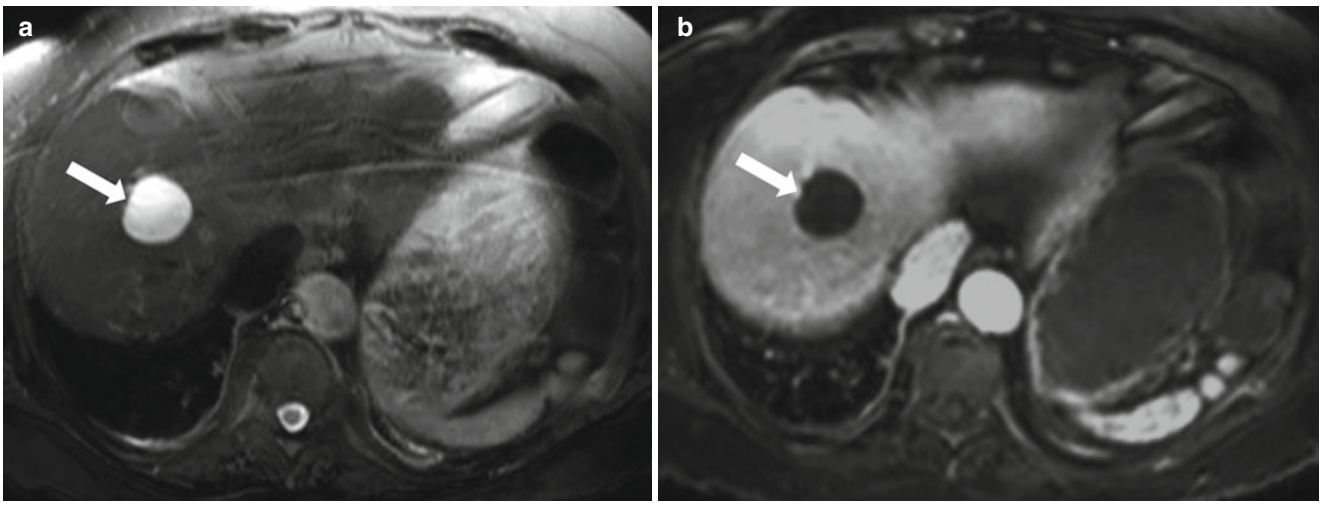

Fig. 2.4 Simple cyst. Axial T2-weighted FSE (**a**), and axial fat suppressed postgadolinium SGE T1-weighted image (**b**). A well-defined lesion that is homogeneously high signal intensity on T2-weighted image (*arrow*) with no enhancement after administration of gadolinium (*arrow*), consistent with simple liver cyst

Key Teaching Points of Cystic Liver Lesions
(Algorithm 2.2)
Definition of simple cystic pattern: a well-circumscribed lesion with a fluid attenuation/signal intensity demonstrating thin wall, with no complex features such as altered content (proteinaceous secondary to infection or hemorrhagic), peripheral enhancement, solid component, calcifications, or septations.

Sporadic simple cyst represents the most common lesion with simple cystic features. Simple cysts can be multiple. Multiple cysts/cyst-like lesions can be seen in ADPKD (commonly associated with renal cysts which can frequently bleed) and biliary hamartomas where subcentimeter simple cystic-looking lesions are noted which are noncommunicating with the biliary tree. On cross-sectional imaging, Caroli disease is characterized by larger cystic-looking lesions communicating with the biliary tree. Very rarely, pancreatic pseudocysts can occur in the liver mimicking simple cysts.

Complex cystic lesions include biliary cystadenoma/cystadenocarcinoma, abscess (clinical and laboratory findings), hematoma (CT attenuation and MR signal intensity of blood degradation products), post RF ablation cavity (can mimic cystic lesion, history of treatment, occasional rim enhancement), and hydatid cysts [occur in endemic areas and could have daughter cysts, calcification, and floating membranes]. Metastases can rarely appear cystic (simple or complex), especially the ones secondary to mucinous tumors and GIST as well as hypervascular metastases which can undergo cystic changes with chemotherapy such as neuroendocrine tumors.

Simple Hepatic Cysts

Hepatic cysts are common liver lesions. Pathogenesis of these cysts is not clear, and acquired cysts are thought to represent retention cysts of bile ductule derivation [3]. The cyst is typically lined with a single layer of cuboidal to columnar epithelial cells. On imaging, cysts are homogeneous and well circumscribed and possess a sharp margin with the liver, with no visible wall. Although slight variations are common, cysts are usually rounded or oval shaped [4].

Simple cysts are fluid attenuation on CT (demonstrating an attenuation <20 HU) with a thin wall and no significant post-contrast enhancement. On MRI, these demonstrate low signal intensity on T1-weighted images and high signal intensity on T2-weighted images, with retention of the high signal intensity on the longer echo time (e.g., TE ≥120 ms) T2-weighted images. Simple cysts should not enhance following intravenous contrast administration (Fig. 2.4). The presence of thick walls or enhancing internal components suggests the diagnosis of hepatic abscess or neoplasm rather than a simple cyst. In addition, simple cyst can be differentiated from cystic metastases using the delayed phase of contrast enhancement where metastases can show enhancement, while cysts do not [5]. Rarely, hemorrhage or infection can complicate cysts, and these account for difficulty in differentiation from other complex cystic lesions including abscesses and neoplasms.

Autosomal Dominant Polycystic Kidney Disease (ADPKD)

Liver involvement is the most frequent extrarenal manifestation in autosomal dominant polycystic kidney disease [6]. Liver cysts are the most frequently encountered manifestation,

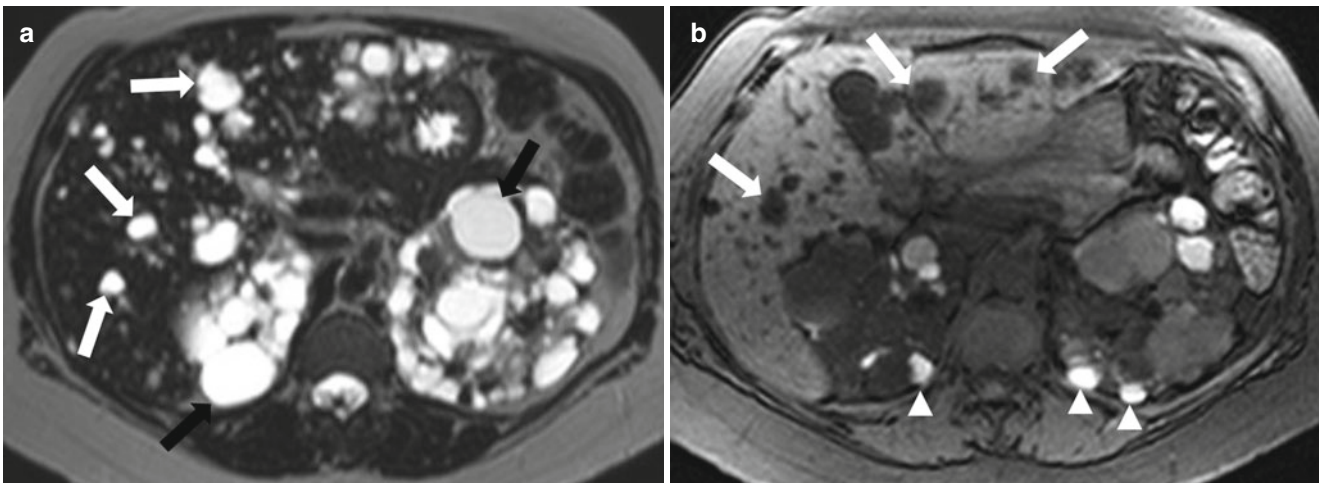

Fig. 2.5 Autosomal dominant polycystic kidney disease. Axial T2-weighted image (**a**), and axial T1-weighted fat-saturated image without intravenous contrast (**b**) demonstrate numerous cysts of varying sizes scattered throughout the liver and kidneys exhibiting high signal intensity on T2-weighted image (*arrows*), with increased signal intensity of some of renal cysts on T1-weighted image (*arrowheads*) indicating hemorrhage. Note that the liver cystic lesions do not communicate with the biliary tree

but other pathologies can occasionally be encountered, including congenital hepatic fibrosis and segmental dilation of the biliary tract. Cysts are usually multiple, with variable sizes (Fig. 2.5), and associated cysts in the kidneys or pancreas and positive family history are helpful in reaching the diagnosis.

Patients with autosomal dominant polycystic liver disease are usually asymptomatic, and severe symptoms can occur in 20 % of patients who develop massive hepatomegaly with compression of the surrounding organs. Rarely, acute complications can be caused by torsion, intracystic hemorrhage, and infections, with liver dysfunction occurring only sporadically [7]. However, advanced disease can result in liver failure, or Budd–Chiari syndrome.

Cysts demonstrate typical features of fluid-containing well-circumscribed lesions with fluid attenuation on CT (manifested by attenuation <20 HU) and MRI (manifested by low signal intensity of T1-weighted and high signal intensity on T2-weighted images) with no significant enhancement on postcontrast series. Because of the larger number of cysts, intracystic hemorrhage is more frequently encountered than in cases of simple hepatic cysts [8]. Intracystic hemorrhage is usually seen as areas of higher attenuation on CT and areas of altered MRI signal intensities due to blood degradation products [9].

Biliary Hamartoma

Biliary hamartoma (also known as von Meyenburg complexes) are benign biliary malformations which are categorized under the spectrum of fibro-polycystic diseases of the liver. They arise from bile duct embryological remnant due to anomalous development of the ductal plate [10]. Biliary hamartomas is not uncommon and occurs in approximately 3 % of patients. These can be solitary or more commonly multiple, and multiple lesions can be extensive.

On CT and MR images, lesions are uniformly small (usually <1.5 cm) and well defined. On CT, the lesions may not be well characterized due to the too small size which may preclude accurate characterization [11]. The fluid content renders these lesions high signal intensity on T2-weighted images and low signal intensity on T1- weighted images. On heavily T2-weighted images, the signal intensity increases further, similar to that of fluid on T2-weighted images.

On MR cholangiography, bile duct hamartomas appear as multiple tiny cystic lesions that do not communicate with the biliary tree [10].

Although this appearance resembles simple cysts, biliary hamartomas may demonstrate a subtle thin rim of enhancement on postcontrast images (Fig. 2.6) due to enhancing fibrous capsule and/or compressed surrounding parenchyma. This rim of subtle enhancement should not be mistaken for other diagnoses such as abscesses and metastases. Capsule can also demonstrate low signal intensity on T2-weighted images.

Caroli Disease

Caroli disease is a rare autosomal recessive condition characterized by congenital cystic dilation of the intrahepatic bile ducts [12]. Although Caroli disease generally involves the entire liver, it may be segmental or lobar. Two forms of Caroli disease have been described: (a) a less common "pure" form (type 1) and (b) a more complex form (type 2) that is associated with other ductal plate abnormalities such as hepatic fibrosis [13].

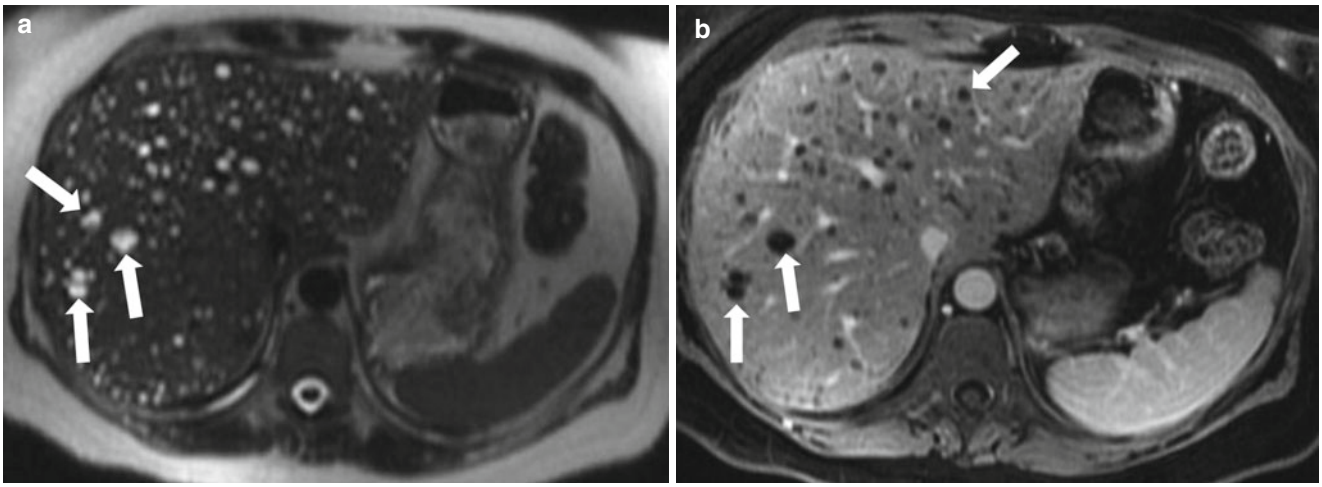

Fig. 2.6 Biliary hamartomas. Axial T2-weighted HASTE (**a**) and axial contrast-enhanced 3D GRE T1-weighted image (**b**) show multiple small lesions representing demonstrating high signal intensity on T2-weighted image (*A*) and low signal intensity onT1-weighted with a thin rim of enhancement (*arrows*). On MRCP (*not shown*), these do not communicate with biliary tree

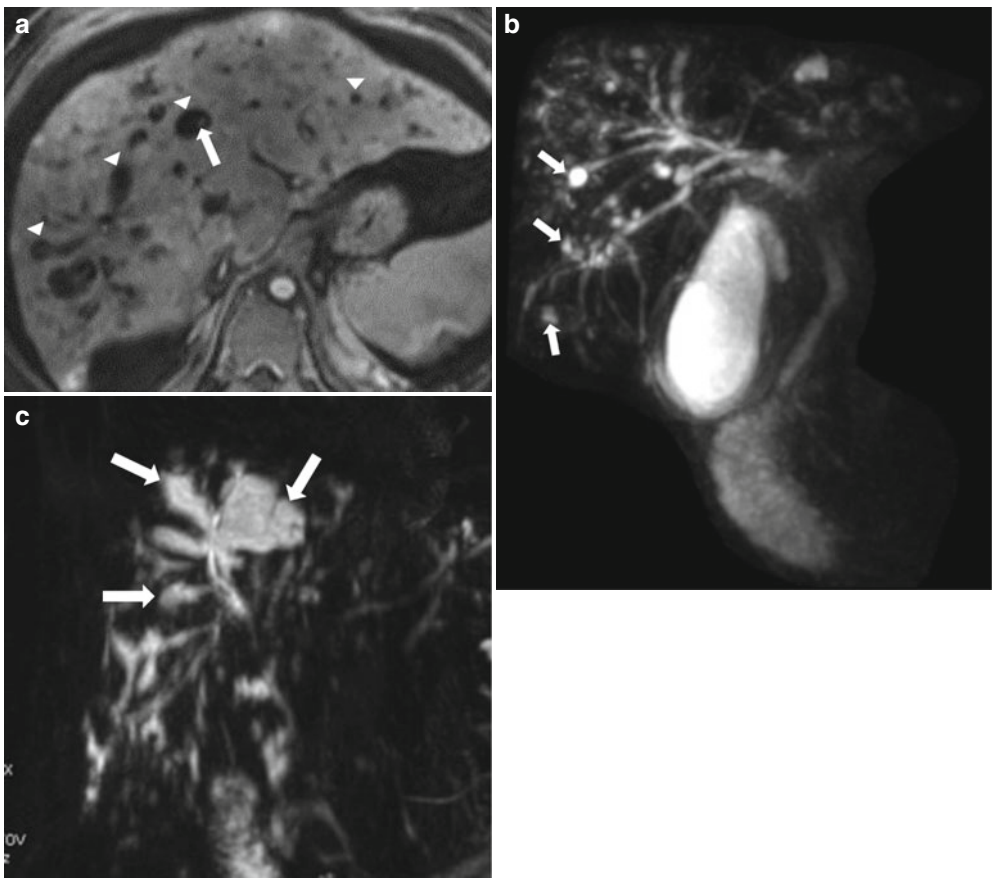

Fig. 2.7 Caroli disease in three different patients, Axial contrast enhanced T1-weighted image (**a**) demonstrating numerous cyst-like lesions (*arrowheads*) with a central tiny enhancing focus (*arrow*), consistent with central dot sign classic for Caroli disease. Coronal MR cholangiogram (**b**) in a 54-year-old male patient, shows saccular dilatation of the biliary tree (*arrows*). Coronal projection MR cholangiogram (**c**) in a 21-year-old female shows a connection between the saccular dilated segmental bile ducts (*arrows*) and the central biliary tree

Often, patients clinically present with bouts of recurrent fever and right upper quadrant pain. Jaundice may occur if the calculi obstruct the common bile duct. On cross-sectional CT and MRI, Caroli disease appears as multiple variable-sized, non-enhancing cystic lesions. MR cholangiopancreatography is a noninvasive imaging technique that has become the first-choice modality for diagnosing Caroli disease [14]. MRCP demonstrates the connection of these cysts to the biliary ducts (Fig. 2.7), which is the key feature for the diagnosis.

The central dot sign is described on contrast-enhanced CT and MRI as well as color Doppler ultrasound as a tiny enhancing focus in the center of cystic-appearing morphology and is

due to the contrast-enhanced small portal venous branch protruding into the dilated intrahepatic bile ducts. This sign has been used to make a diagnosis of Caroli disease [15].

Complications may occur secondary to bile stagnation which leads to cholangitis and formation of calculi which may result in biliary obstruction and jaundice. Cholangiocarcinoma has been reported to complicate Caroli disease in 7 % of cases [16].

Complex Cystic Lesions

These are predominantly cystic lesions, yet with complex features such as septations, calcification, or peripheral enhancement. Altered fluid content is another feature of complexity including proteinaceous fluid secondary to infection or hemorrhagic fluid.

These include:

- Biliary cystadenoma/cystadenocarcinoma
- Complex cyst
- Cystic metastasis
- Abscess
- Hydatid cyst
- Hematoma
- Post RF ablation cavity

Other less common causes include: intrahepatic biloma and undifferentiated sarcoma.

Biliary Cystadenoma/Cystadenocarcinoma

Biliary cystadenoma/cystadenocarcinoma is a group of rare biliary neoplasms occurring most commonly in middle-aged women. Biliary cystadenomas are considered premalignant neoplasms with the majority located in the liver with a significantly less incidence in the extrahepatic biliary tree. These are often incidental, but symptoms can arise due to mass effect of large lesions.

Typically, these tumors appear as multiloculated lobulated cystic lesions with several septations and occasional solid nodules. On CT and MR imaging, these appear as cystic (typical fluid characteristics on CT and MRI), with enhancing septations and solid components [17]. Wall or septal calcifications can be also seen. Altered characteristics of the fluid can be seen due to mucin/protein contents or hemorrhage. These can be demonstrated as higher CT attenuation and higher signal intensity on T1-weighted images (Fig. 2.8) [18].

Although malignant tumors tend to have thicker nodular septations, there is no definite reliable criterion for differentiating cystadenoma from cystadenocarcinoma as nodular soft tissue projections can be seen in both tumors [19].

Liver Abscess

Bacterial infection is the most common cause of liver infectious processes leading to the formation of pyogenic abscesses. These can be caused by hematogenous spread particularly if multiple (of either gastrointestinal infection

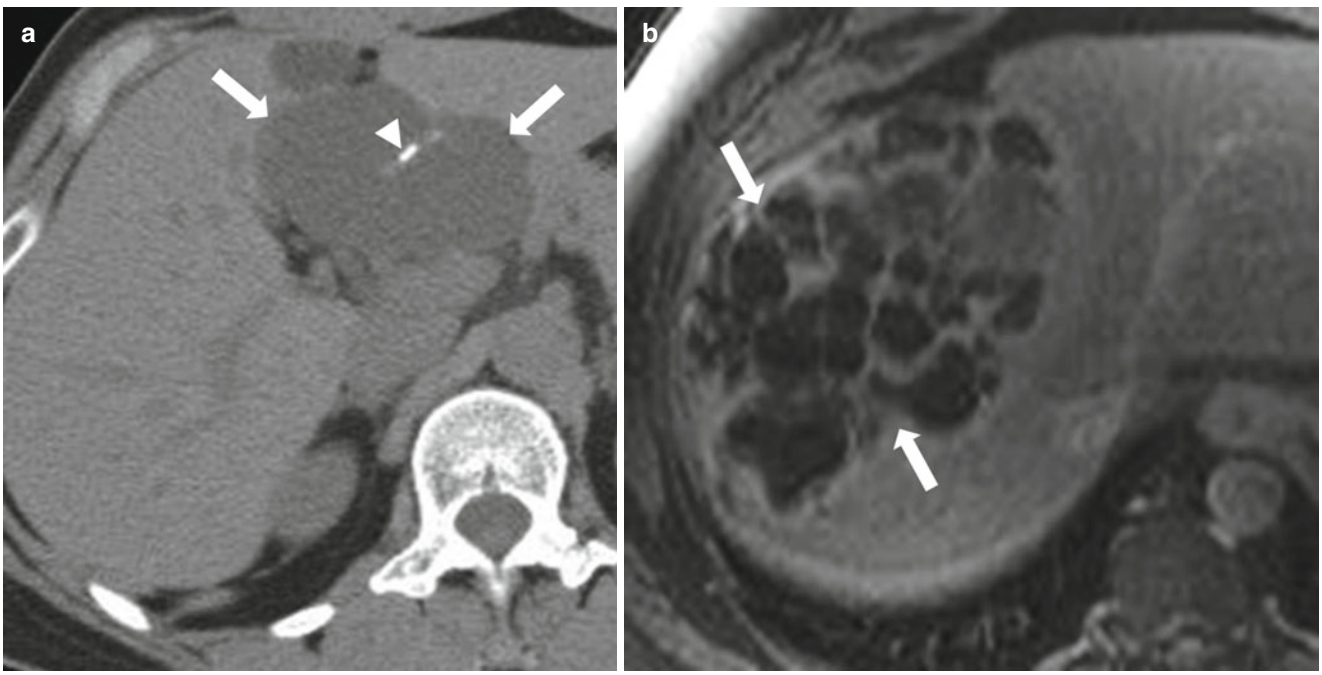

Fig. 2.8 Biliary cystadenoma; Axial nonenhanced CT (**a**) showing multiloculated fluid attenuation lesion (*arrows*) in the left lobe with septal calcifications (*arrowhead*). Axial postcontrast T1-weighted image (**b**) and coronal T2-weighted image HASTE (**c**) in a different patient demonstrate multiloculated cystic lesion in the right lobe (*arrows*), with multiple enhancing septations, consistent with biliary cystadenoma

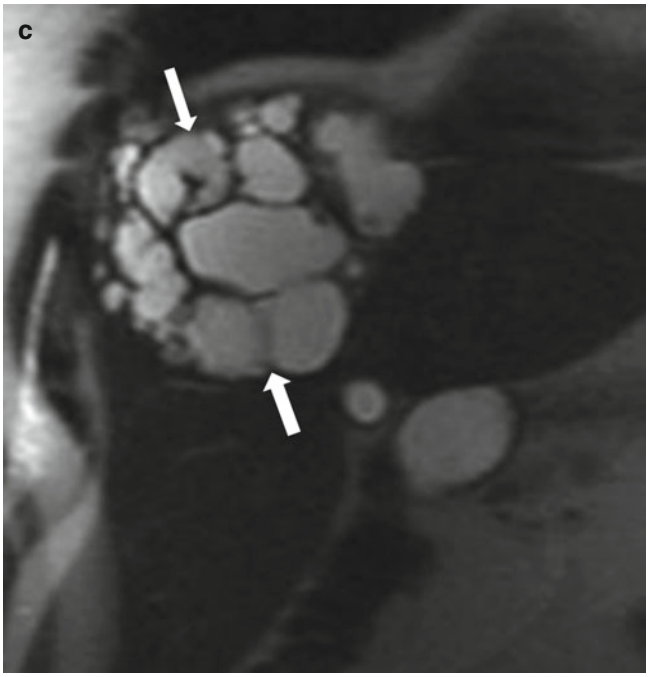

Fig. 2.8 (continued)

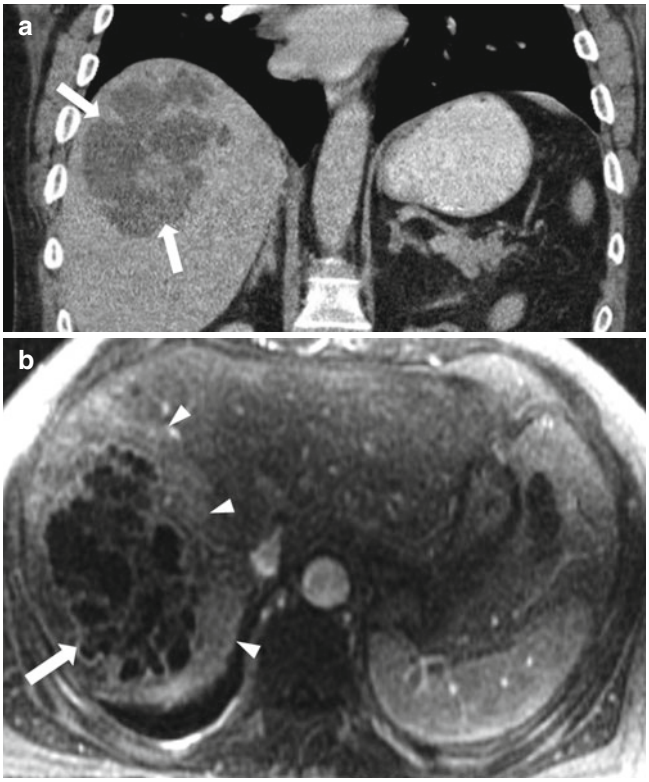

Fig. 2.9 Pyogenic liver abscess; coronal reformatted contrast-enhanced CT (**a**), axial postcontrast-enhanced T1-weighted (**b**) showing large complex multiloculated cystic lesion (*arrows*) with thick enhancing rim and central septations seen within the hepatic dome with perilesional enhancement (*arrowheads*)

via the portal vein or disseminated sepsis via the hepatic artery), ascending cholangitis, or superinfection of necrotic tissue [20–22]. A solitary hepatic abscess is usually cryptogenic and may not have a known etiology [22].

In a more recent report, biliary infection is the most common sources of infection. Clinical presentation includes signs of right upper quadrant pain, tenderness, and hepatomegaly with occasional occurrence of jaundice and pulmonary changes. Symptoms include generalized malaise, fever, and weight loss as well as chills. Liver function tests and total leukocyte count (>10.000) are elevated in most patients [23].

Treatment options include percutaneous drainage, surgical resection, and intravenous antibiotics with a mortality rate of 9.4 % in the surgically treated group and 16.6 % in the nonsurgically treated group [24].

Pyogenic abscess is the most common focal parenchymal lesion due to bacterial infection. Hepatic abscess can be solitary or multiple which may vary from small (few millimeters) to massive lesions. Infectious process usually starts by diffuse inflammatory process but later matures to a well-defined abscess cavity surrounded with fibrous capsule, which gives the abscess the characteristic pattern of early, persistent moderate to intense ring enhancement, without progressive enhancement of the stroma, which – beside the constitutional symptoms – helps to differentiate multiple abscesses from metastases which usually shows progressive stromal enhancement. The central necrotic cavity exhibits low attenuation on CT, low signal intensity on T1-weighted images, high signal on T2-weighted images, and with no significant postgadolinium enhancement. Transient segmental wedge-shaped hepatic enhancement associated with hepatic abscesses are usually seen in the early postcontrast images due to surrounding inflammatory response in the adjacent liver [25, 26], and this perilesional enhancement resolves on delayed images (Fig. 2.9). In the absence of history of intervention, the presence of intralesional gas bubbles, which appears as gas-attenuating regions on CT or signal void foci on MR, is virtually diagnostic for pyogenic abscesses [25, 26].

Amebic abscesses are caused by *Entamoeba histolytica* which is endemic in developing countries such as India, Middle East, Far East, Africa, and South America but can also occur in as immigrants and travelers from these endemic regions, and the condition is typically characterized by diarrhea which is one of the initial symptoms of the disease.

Increased serum antibodies to *Entamoeba* are characteristic in the majority of cases [27]. A single abscess predominantly located in the right lobe with a thick enhancing capsule is characteristic for amebic abscess. Perilesional edema can be also visualized. Chest wall and pleural involvement are also noted in some cases of amebic abscesses.

Hydatid Cyst (Echinococcal Cyst)

Echinococcus granulosus represents the most common organism causing echinococcal disease which is endemic to the Mediterranean basin, Middle East, and other sheep-raising areas [24]. Pathologically, the typical hydatid cyst is

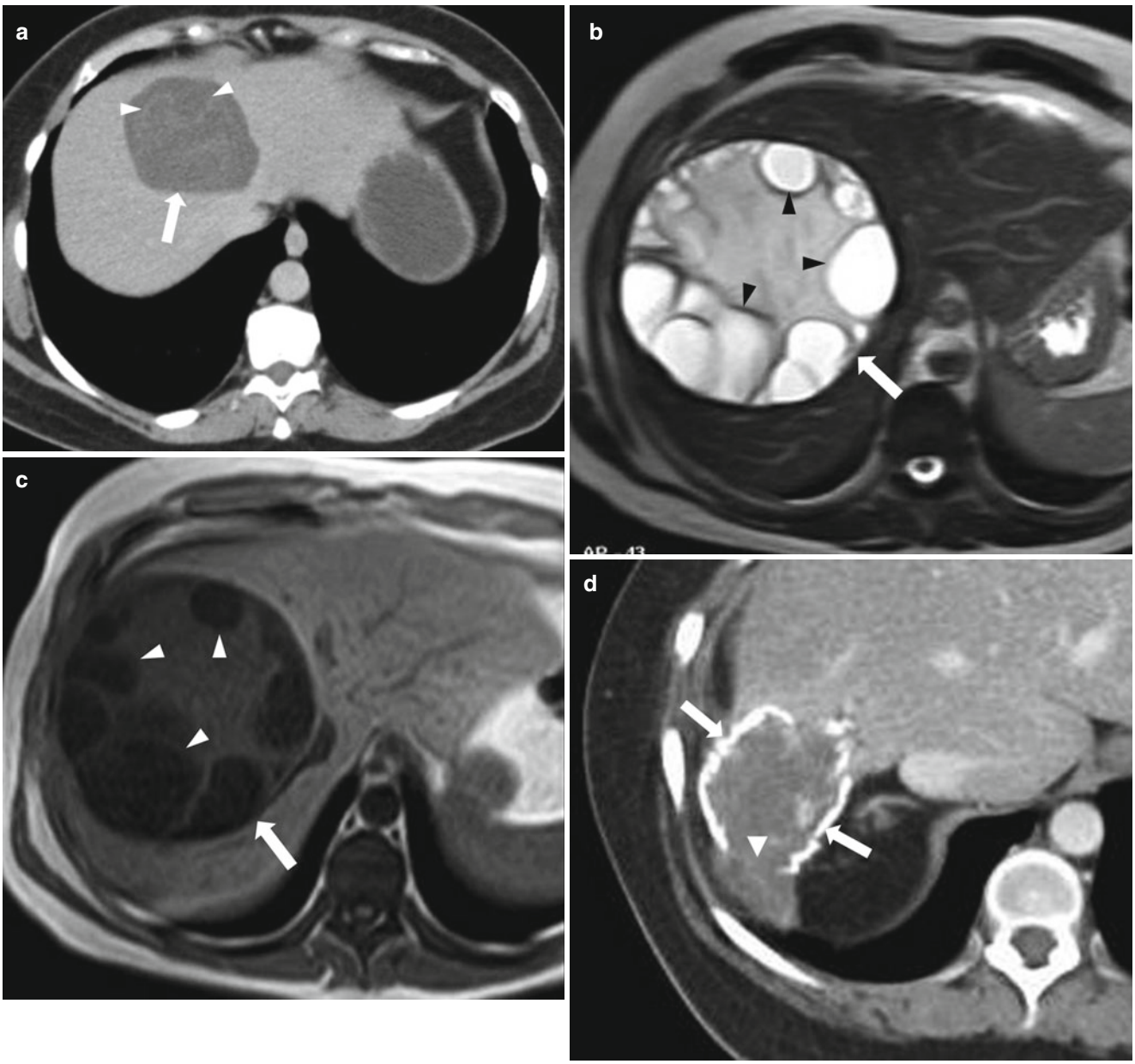

Fig. 2.10 Three different cases of echinococcal cysts; axial contrast-enhanced CT (**a**) demonstrating a well-circumscribed cystic lesion (*arrow*) with water lily sign (irregular thin internal linear floating membranes) (*arrowheads*). Axial T2-weighted image and T1-weighted image, respectively (**b, c**), demonstrating multiple peripheral internal cystic lesions (daughter cysts) (*arrowheads*) within the larger mother cyst (*arrows*). Axial contrast-enhanced CT (**d**) demonstrating a hydatid cyst with wall calcification (*arrows*) which demonstrates focal interruption (*arrowhead*); a sign associated with impending rupture

well circumscribed spherical with a fibrous rim. Surrounding liver reaction to the abscess is minimal, with a small amount of granulation tissue. The typical imaging feature is multicystic lesion with daughter cysts arranged peripherally within the larger cyst. Occasionally, some cysts are seen outside the fibrous capsule of the main hepatic cyst. Typically, cysts have low signal intensity on T1-weighted and high signal intensity on T2-weighted images. Lesions are frequently complex, with mixed high and low signal intensity on T2- and T1-weighted images, respectively, due to the presence of proteinaceous content and cellular debris (Fig. 2.10). The fibrous capsule and internal septations can be well shown on T2-weighted images and gadolinium-enhanced T1-weighted images [28]. Calcification of the cyst wall or content is frequently identified on CT images but difficult to distinguish from the fibrous capsule in MRI due to the low signal intensity of both on T2-weighted images [28]. Interruption of wall calcification represent a sign of impending rupture.

Intrahepatic Hematoma

Hematoma occurs as a result of blunt trauma such as motor vehicle accident, or surgical/interventional procedures

including biopsy, and appears as a fluid collection with varying density/signal intensity depending on the age of the blood products.

On CT, acute hematoma demonstrates high attenuation on precontrast CT with no significant postcontrast enhancement. Attenuation decreases with aging of the blood products. MR imaging is the most sensitive and specific modality for diagnosing hematomas. MR imaging features vary according to the age of the hematoma. In hyperacute stage (<24 h), oxyhemoglobin represents the main component which is demonstrated as simple fluid with low signal intensity on T1-weighted and high signal intensity on T2-weighted images. In the acute stage (1–3 days old), deoxyhemoglobin results in increased paramagnetic susceptibility with low signal intensity on T2-weighted images. Early subacute stage (from day 3 to 7) is characterized by the presence of intracellular methemoglobin which still leads to low signal intensity on T2-weighted and high signal intensity on T1-weighted images. Late subacute stage (day 7–14) is characterized by the presence of extracellular methemoglobin which results in a high signal intensity on T1-weighted and high signal on T2-weighted images (Fig. 2.11). Chronic hematoma (older than 14 days) is characterized by the presence of hemosiderin which results in low signal intensity on T1-weighted and low signal intensity on T2-weighted images [29, 30]. Some hematomas show rim enhancement after contrast material administration [31].

Post Radiofrequency Ablation (RFA) Cavity

In addition to surgical resection, other nonsurgical interventional procedures have been established to treat liver malignancies. These include radiofrequency (RF) ablation, cryoablation, ethanol ablation, microwave ablation, and laser ablation: they all play an important role particularly in the treatment of solitary lesions [32]. Effective treatment is indicated by the decrease in size or at least no change of size of the ablation cavity.

Expected normal findings after ablation include ill-defined perilesional enhancement secondary to inflammatory reaction (up to 6 months after ablation), with a higher than simple fluid attenuation on CT, high signal intensity on T1-weighted images secondary to coagulative necrosis which persists for several months post ablation.

A well-defined marginal enhancement, nodular enhancement, and washout are all concerning for neoplastic residual/recurrence.

The ablated area must exceed the tumor margins by approximately 1.0 cm [33]. Over time, the ablated zone might either shrink or retain similar size to the original lesion [34]. Enlargement of the ablated area on follow-up examinations is suggestive of unsuccessful intervention [35]. In early post-treatment weeks, the signal intensity on T2-weighted and T1-weighted images corresponds to the hemorrhage and either liquefactive or coagulative necrosis [34]. Signs of successful treatment include lack of contrast enhancement. Early after intervention, an ill-defined perilesional rim is often observed that appears mildly high signal intensity on T2-weighted images and exhibits moderate to intense enhancement on arterial dominant-phase images [34, 35]. Over time, thickness of the perilesional rim regresses in successfully treated lesions and gradually disappears several months after ablation (Fig. 2.12) [33]. The perilesional rim corresponds to intense inflammatory reaction and hemorrhage, which are gradually replaced by granulation tissue [33].

The presence of a nodular focus of high intensity in T2-weighted images and nodular enhancement mainly in the

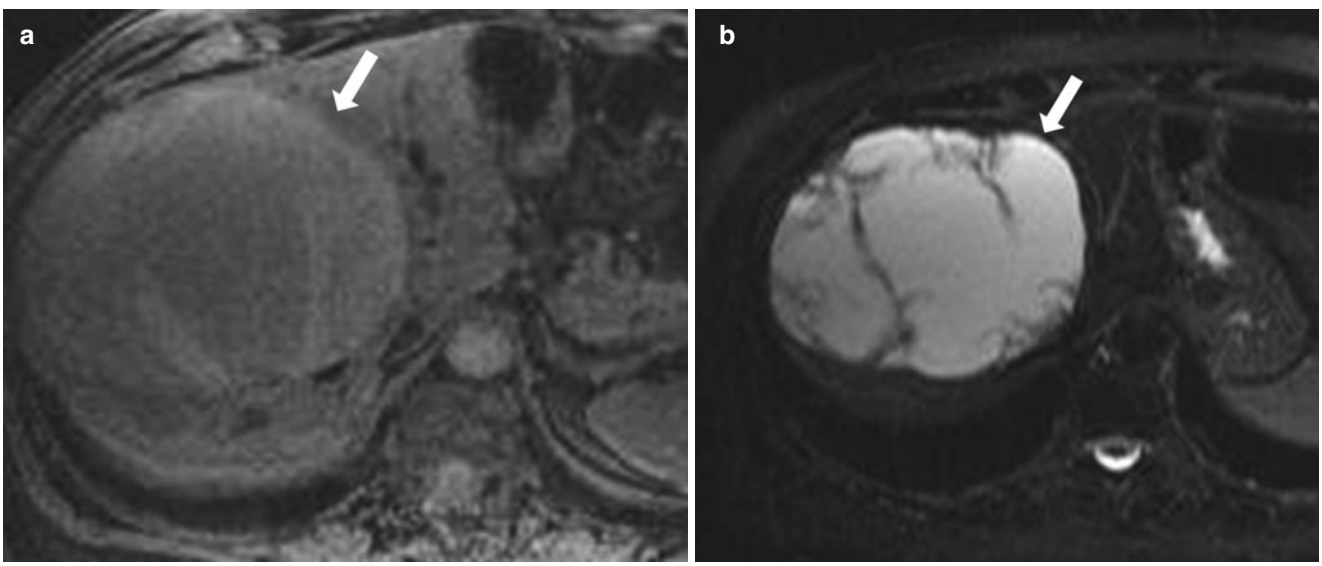

Fig. 2.11 Axial T1-weighted image (**a**) and axial T2-weighted image (**b**) demonstrate ovoid shaped weel-circumscribed lesion (*arrows*) exhibiting intermediate to high signal intensity on T1-weighted and high signal intensity on T2-weighted images, consistent with subacute hematoma. Note thick fibrous capsule, intralesional septations, and underlying liver parenchymal displacement.

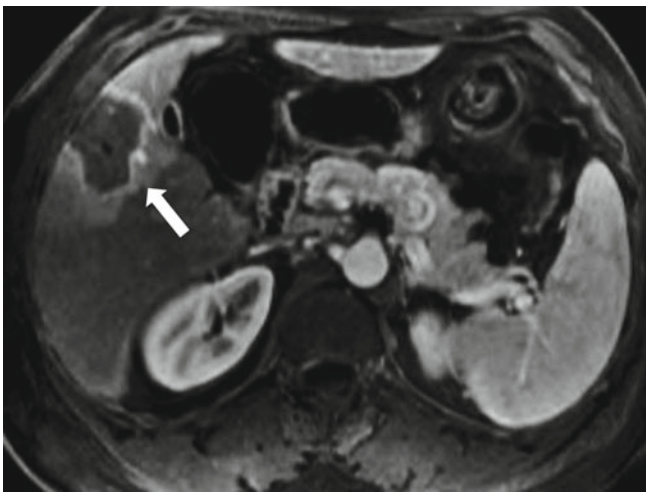

Fig. 2.12 Axial contrast enhanced T1-weighted image one month following radio-frequency ablation demonstrates a low signal intensity cavity with a peripheral smooth uniform enhancement (*aroows*), this pattern is normally seen in early few months after radiofrequency ablation

arterial phase is indicative of residual or recurrent tumor (Fig. 2.13) [33, 34], which may washout on late-phase images.

Cystic Metastases

A minority of liver metastases can be cystic which can lead to diagnostic dilemma as these can be confused with the more common benign cystic lesions. Occasionally, gastrointestinal stromal tumor (GIST) and mucinous adenocarcinoma of the colon or ovary can result in cystic liver metastases. Rapidly growing metastases secondary to hypervascular tumors can overgrow their blood supply leading to cystic degeneration and necrosis. Examples of these tumors include neuroendocrine tumors, melanoma, and breast carcinoma. These lesions often demonstrate fluid attenuation on CT (Fig. 2.14). On MRI, low signal intensity on T1-weighted images and high signal intensity on T2-weighted images are noted. On postcontrast series, peripheral rim-like enhancement can be seen on early phases with occasional gradual filling on delayed phase. Knowledge of the clinical history can help in the differential diagnosis. Cystic metastases can be active or inactive (particularly in those which develop cystic changes secondary to treatment). PET scan can be also utilized and often demonstrate increased FDG uptake with active cystic metastases which differentiates them from the more common benign cystic lesions [18, 36–39].

Intrahepatic Pseudocyst

Intrahepatic or subcapsular pseudocysts are rare cystic lesions that can develop in the setting of pancreatitis which may dissect into the liver along portal triads (Fig. 2.15), leading to subjacent collection which further results in the formation of pseudocyst. The clue for the intrahepatic pseudocyst is the clinical presentation in addition to other imaging features of pancreatitis.

Other less common cystic lesions include:

- Intrahepatic Biloma (related to biliary tree, secondary to trauma, or after an interventional or surgical procedure): Excretion of contrast into the biloma is demonstrated on 20 min after MR hepatobiliary contrast administration, proving that it communicates with the bile ducts.
- Undifferentiated Embryonal Sarcoma: Rare malignant tumor occurring in older children (mean age 12 years) may contain calcifications and solid component.

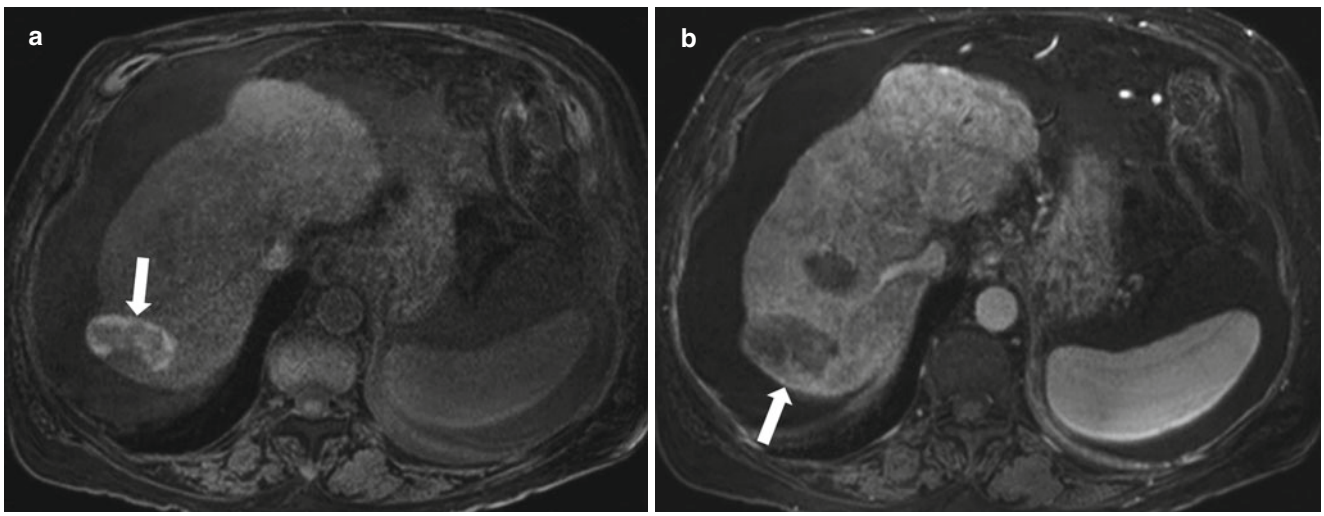

Fig. 2.13 Axial precontrast T1 weighted (**a**) and contrast enhanced T1 weighted (**b**) images demonstrating a post ablation cavity showing high signal intensity(coagulative necrosis) on T1-weighted image (*arrow in* **a**), with a nodular peripheral enhancement (*arrow in* **b**) in the arterial phase denoting residual/recurrent tumor

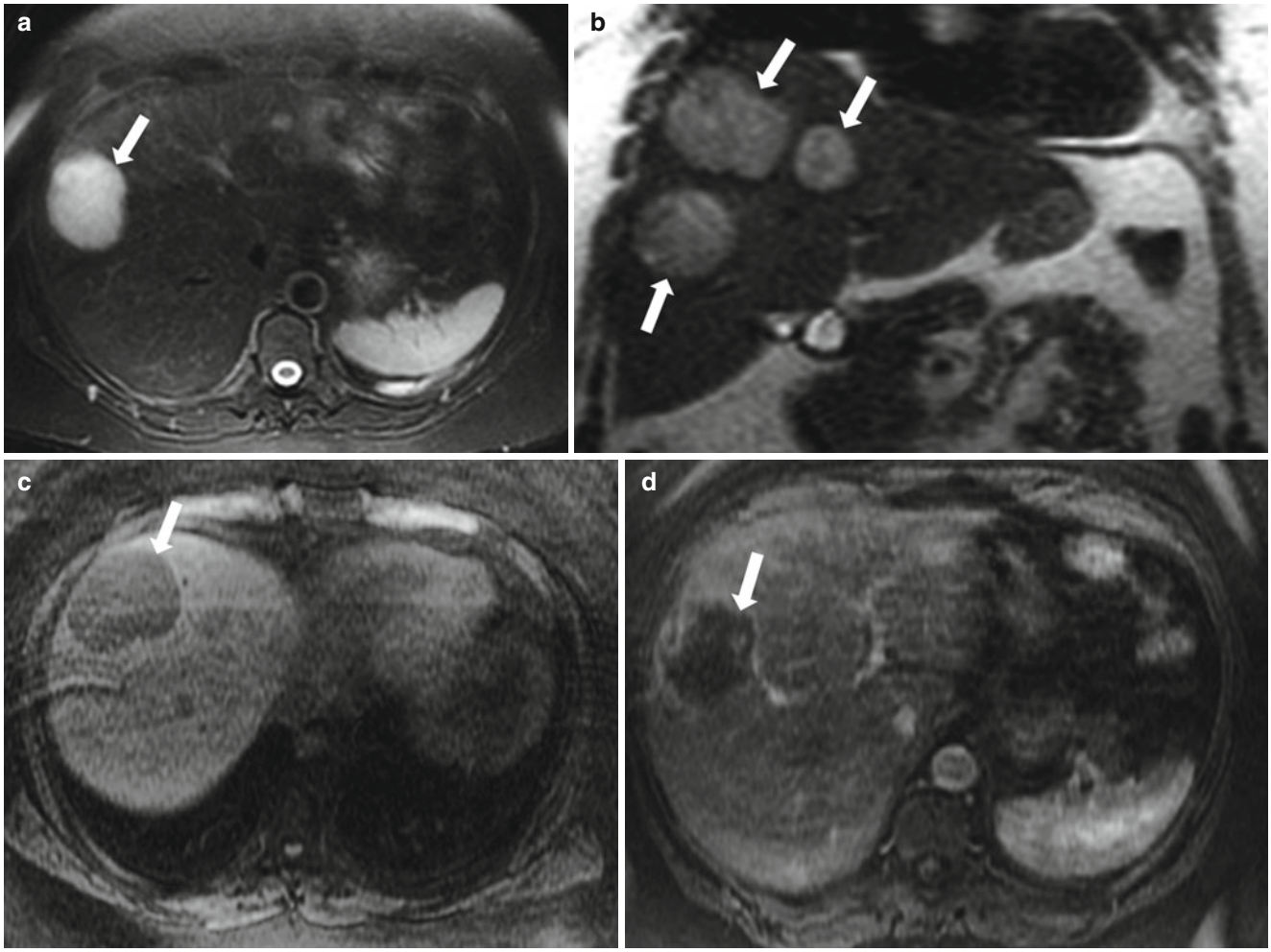

Fig. 2.14 Cystic metastasis secondary to neuroendocrine tumor. Axial T2-weighted with fat suppression (**a**), coronal T2-weighted (**b**), axial non-enhanced T1-weighted (**c**) and axial contrast enhanced T1-weighted (**d**) images demonstrate well circumscribed cystic lesions (*arrows*) demonstrating low signal intensity on T1-weighted image, markedly increased signal intensity on T2-weighted images with a slight peripheral enhancement on post-contrast images. These represented cystic metastatic lesions in a 60 year old female with metastatic neuroendocrine tumor 60 year old female with metastatic neuroendocrine tumor

Fig. 2.15 Pseudocyst. Axial contrast-enhanced CT demonstrates a well-defined fluid attenuation lesion (*arrow*, representing pseudocyst in the liver hilum (*arrow*) in a 76-year-old man with recurrent pancreatitis

Hypoenhancing Lesions (Algorithm 2.3)

Hypoenhancing lesions show mild enhancement after intravenous contrast injection. This enhancement is, however, less than the background liver. For this reason, these lesions appear hypodense on contrast-enhanced CT and hypointense on contrast-enhanced T1-weighted images. Other lesions such as focal fatty infiltration may appear similarly hypodense on CT and hypointense on contrast-enhanced T1-weighted *mimicking hypoenhancing mass lesions* (this can be differentiated by drop of signal intensity on out of phase compared to in phase and will be discussed under lesions containing intracellular lipid).

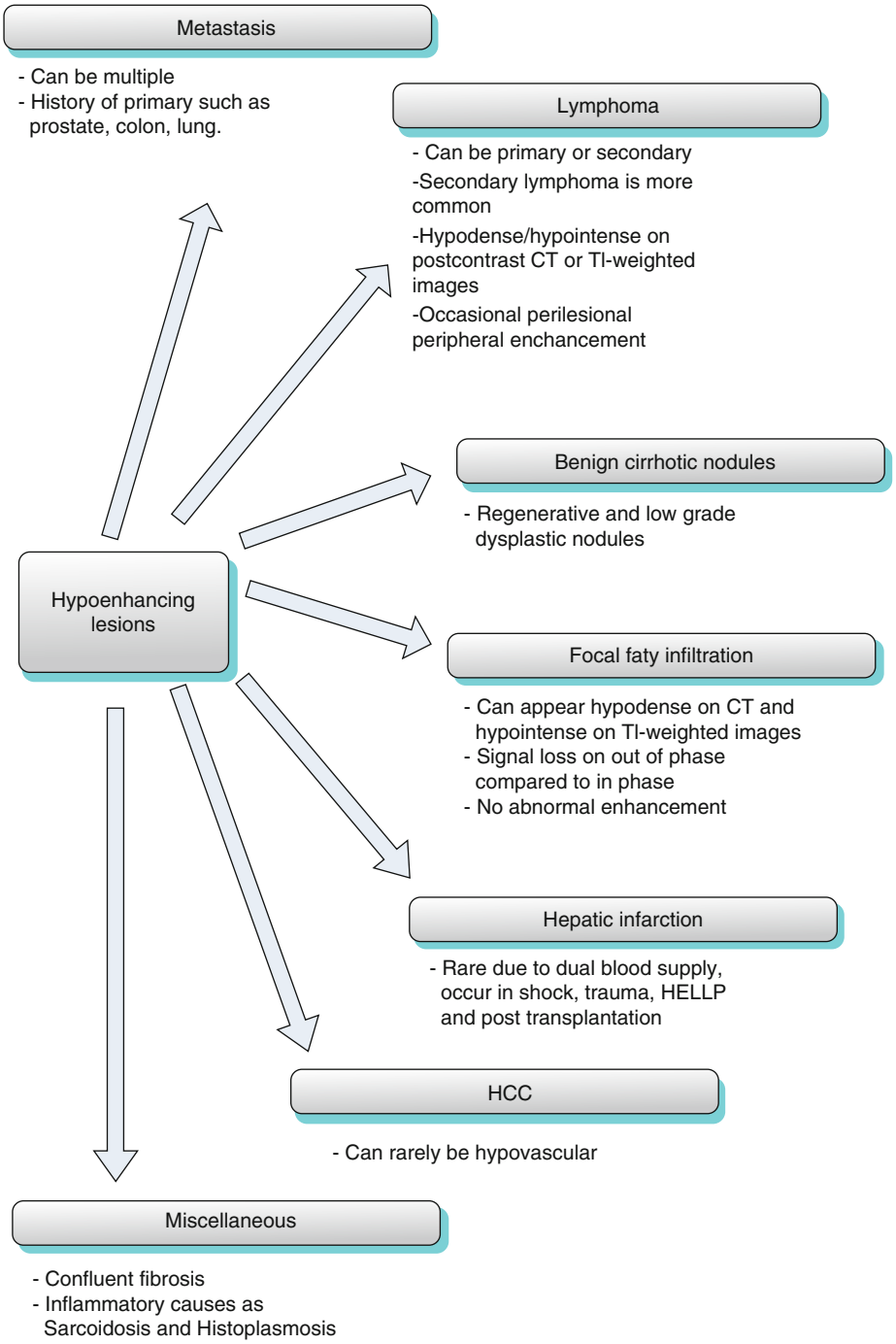

Algorithm 2.3 Algorithm for the hypoenhancing lesions

Regenerative Nodules (Benign Cirrhotic Nodules)

Regenerative nodules are best seen and evaluated by MRI, the majority of the regenerative nodules are hypodense/isodense on CT and hypo-/isointense on T1-weighted images, and in some occasions, regenerative nodules appear low signal in T2-weighted images compared to the background high signal [40]. In 16 % of cases, regenerative nodules appear hyperintense on T1-weighted images which is related to high-protein content. Some of these nodules contain iron, hence the name siderotic nodules; these appear of high density on precontrast CT with low signal intensity of T1-weighted images and low signal intensity and blooming on T2-weighted images (Fig. 2.16). As regenerative nodules maintain portal venous blood supply with minimal if any hepatic artery supply, they enhance minimally (Fig. 2.17) on the hepatic arterial dominant-phase images and thus appear relatively hypointense/isointense to the liver on MRI or hypodense/isodense on CT compared to the enhancing surrounding liver parenchyma [41].

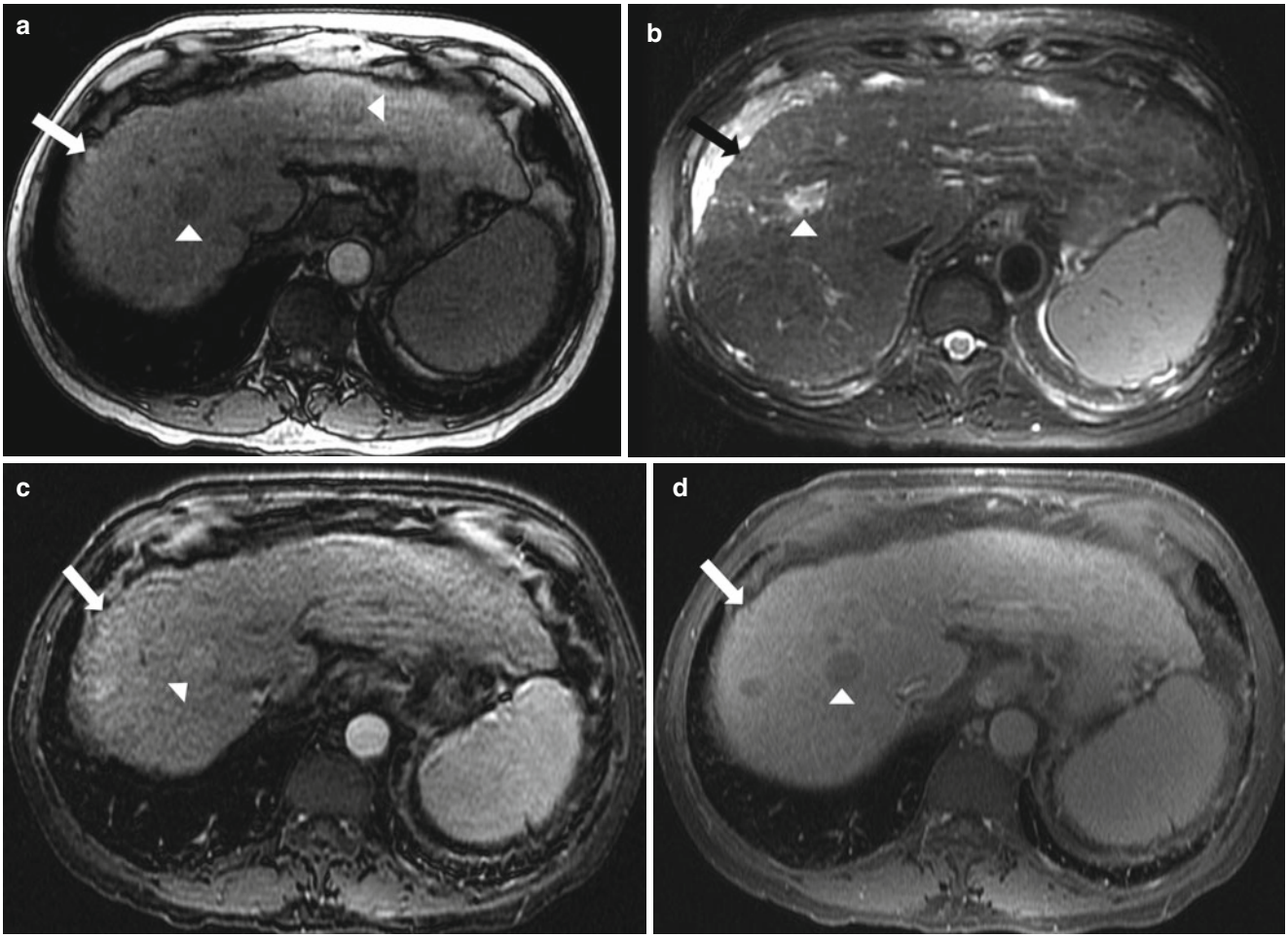

Fig. 2.16 Regenerative cirrhotic nodule. Axial nonenhanced T1-weighted (**a**), axial T2-weighted (**b**), axial contrast enhanced T1-weighted in arterial (**c**), and delayed phase (**d**) demonstrate high signal intensity on nonenhanced T1-weighted image (*arrow* in **a**) which becomes isointense to the liver on T2-weighted image and after intravenous contrast (*arrow* in **b, c** and **d**), representing regenerating nodule. Foci of hepatocellular carcinoma are also noted (*arrowheads*) demonstrating low signal intensity on nonenhanced T1-weighted image, high signal intensity on T2-weighted images, with homogeneous enhancement on arterial phase and washout on delayed postcontrast phase.

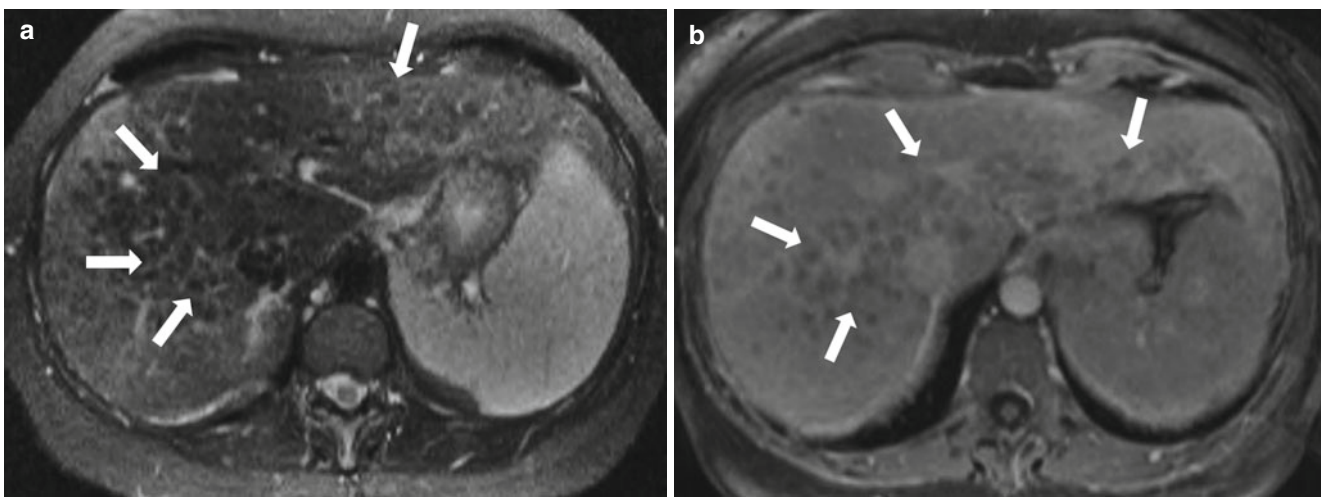

Fig. 2.17 **Regenerative siderotic nodules**. Axial fat-saturated T2-weighted image (**a**) and contrast enhanced T1-weighted image (**b**) demonstrating coarse nodular contour of the liver with numerous nodules (*arrows*) appearing hypointense relative to the liver parenchyma on T2-weighted and contrast enhanced T1-weighted images, consistent with regenerative nodules

Hepatic Infarction

Liver infarction is rare, and this rare incidence is due to dual blood supply to the liver. Infarction can however occur in settings of shock, trauma, HELLP (hemolysis, elevated liver enzymes, low platelets), and post-transplantation (Fig. 2.18). The classic appearance is a peripheral wedge-shaped areas of low attenuation on CT, low signal intensity on T1-weighted, and high signal intensity on T2-weighted images with less enhancement compared with the surrounding liver parenchyma on postcontrast series.

Sarcoidosis

Sarcoidosis is an idiopathic systemic inflammatory granulomatous disease. It affects the lymph nodes, lung, and liver in descending order of frequency. Histologically, the liver is affected in majority of patients, but clinical or radiological manifestations are less evident [42]. Liver involvement can be diffuse or focal with associated enlarged retroperitoneal lymph nodes. On CT, sarcoidosis can be visualized as innumerable small hypoattenuating lesions (Swiss cheese pattern), which enhance less than the liver parenchyma on postcontrast CT. On MR, the diffuse pattern appears as an enlarged heterogeneous liver, while the focal pattern appears as a multiple, small nodules exhibiting low signal intensity on T1- and T2-weighted images. After IV contrast administration, these demonstrate enhancement less than the surrounding parenchyma and could demonstrate some enhancement on the delayed phase (Fig. 2.19) [43].

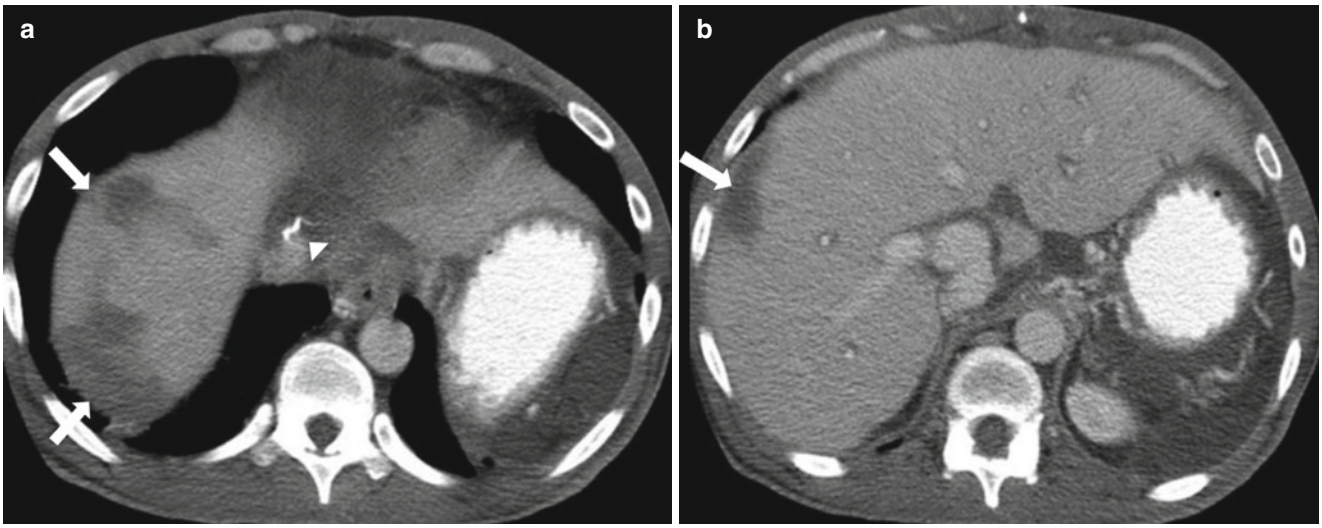

Fig. 2.18 Post-transplant liver infarcts. Axial contrast-enhanced CT for evaluation of post-liver transplant, demonstrating peripheral wedge-shaped low-attenuation areas (*arrows*) in the periphery of right hepatic lobe of the liver consistent with posttransplantation infarcts. Surgical sutures (*arrowhead* in **a**) are noted related to IVC.

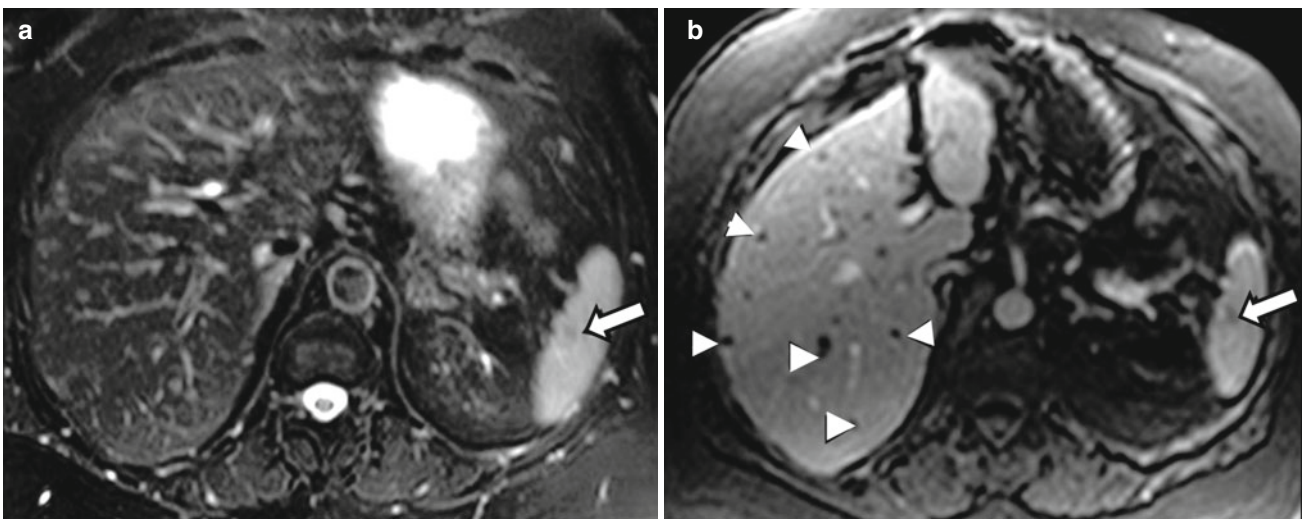

Fig. 2.19 Sarcoidosis. Axial T2-weighted image (**a**) and axial contrast enhanced T1-weighted image (**b**), demonstrating several small hepatic lesions (*arrowheads*) with low signal intensity on both T2-weighted and contrast enhanced T1-weighted images. similar nodule is noted in the spleen (*arrow*).

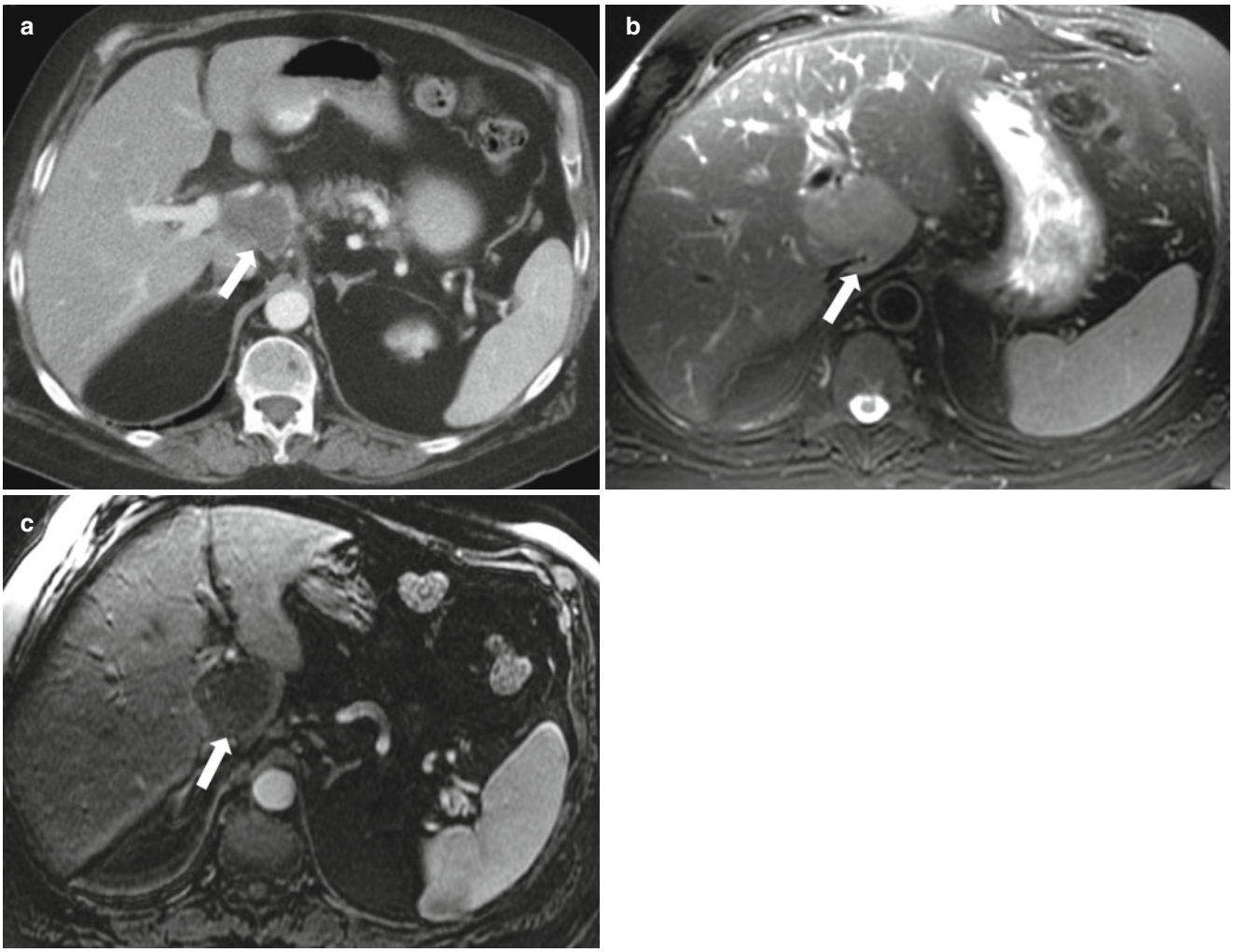

Fig. 2.20 Hepatic lymphoma. Axial contrast enhanced CT (**a**), axial T2-weighted (**b**) and contrast enhanced T1-weigted (**c**) demonstrate a well circumscribed hypoattenuating on contrast enhanced CT, mildly increased signal intensity on T2-w and low signal intensity on contrast enhanced T1-weighted images. The mass abuts the portal vein, hepatic artery, and common bile duct with no evidence of vascular or biliary ductal obstruction

[Swiss cheese pattern (innumerable small holes) is characteristic for sarcoidosis but can be also seen with candidiasis, TB, and metastases. The spleen is typically involved in sarcoidosis and candidiasis.]

Lymphoma

Secondary hepatic lymphoma is considerably more common than primary involvement, and the majority are non-Hodgkin lymphomas. Most tumors usually present as a large solitary mass, but they may vary in appearance from multiple nodules to diffuse involvement. Secondary involvement of the liver by lymphoma is common in stage IV disease [44]. On imaging, lesions vary in signal intensity from low to moderately high on T2-weighted images and are typically low in signal intensity on T1-weighted images and tend to enhance minimally in the postcontrast sequences, leading to hypointense signal intensity relative to the surrounding enhancing liver parenchyma. Enhancement on immediate postcontrast images usually is predominantly peripheral. Lesions of malignant lymphoma may possess transient, ill-defined perilesional enhancement on postgadolinium images (Fig. 2.20) [45].

Focal Infectious Parenchymal Disease

Inflammation/Infection

As previously stated, infectious process usually starts by diffuse inflammatory process but later matures to well-defined abscess cavity. If imaged at that early stage (before formation of abscess), this area of focal inflammation demonstrates patchy ill-defined hypodense area on CT and demonstrates low signal intensity on T1-weighted images and high signal intensity on T2-weighted images with enhancement less than the surrounding liver parenchyma.

Algorithm 2.4 Several pathologies can demonstrate peripheral (or what is called "ring") enhancement. The main entities demonstrating this pattern include metastasis, and abscess. Metastasis usually washes out in delayed phase, but abscess does not wash out. RFA cavity can demonstrate ring enhancement which is a normal finding that can persist several months after the procedure

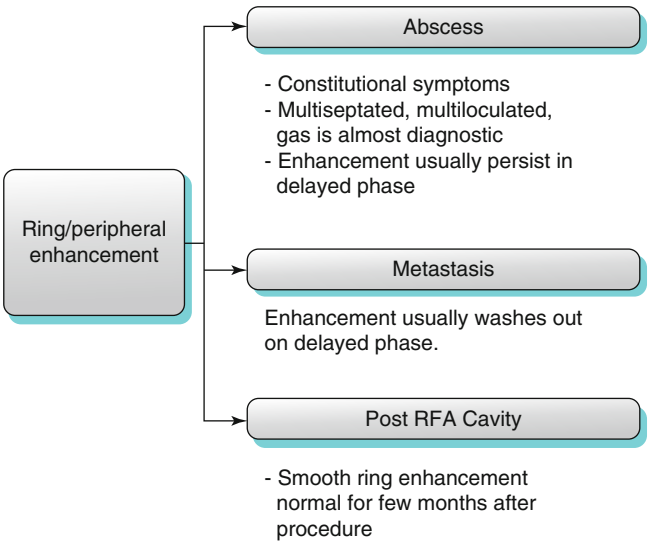

Liver Metastases

Metastases are far more common than primary malignant tumors of the liver, especially in the developed countries.

Various imaging patterns have been described for liver metastases; for descriptive purposes, these can be classified into:

- Hypoenhancing: lesions demonstrating lesser enhancement than the surrounding liver parenchyma
- Hyperenhancing: lesions demonstrating greater enhancement than the surrounding liver parenchyma
- Cystic/necrotic: as previously described in the section of cystic lesions
- Peripheral/ring enhancement (Algorithm 2.4)

Liver metastases are usually multiple and can have variable sizes and appearances.

T2-weighted images with fat-suppression and diffusion-weighted images are very important sequences in detecting liver metastases. This is particularly important in patients with fatty liver where small lesions can be easily missed in the non-fat-suppressed sequences due to relatively increased signal intensity of the liver [46]. Liver metastases are usually hypodense on precontrast CT, hypointense on T1-weighted images, and hyperintense on T2-weighted images and demonstrate various patterns of enhancement in the postcontrast sequences.

- Peripheral enhancement is a characteristic pattern of enhancement in early phase after intravenous contrast administration phase (Fig. 2.19) [47], which can be typically described as peripheral early enhancement with or without progressive centripetal filling in the delayed phase. This pattern of peripheral enhancement could correlate to the highly vascularized outer portion of the tumor. In delayed phase, the center may enhance with occasional washout of the periphery (Fig. 2.21) [47, 48].
- Hypoenhancing Metastases: Some metastases enhance less than the surrounding liver parenchyma and thus appear hypodense relative to the surrounding liver parenchyma on contrast-enhanced CT and hypointense on contrast-enhanced T1-weighted images. Common primary tumors resulting in this pattern include the lung, gastrointestinal tract, prostate, transitional cell carcinoma, and breast (Fig. 2.22) [49]. Hypoenhancing metastases demonstrates minimal enhancement on arterial phase that can be

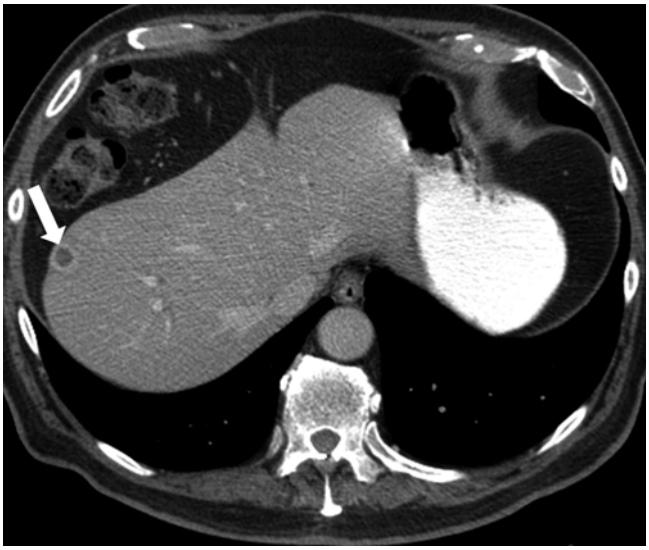

Fig. 2.21 Axial contrast-enhanced CT demonstrates a peripherally enhancing lesion (*arrow*) within segment VIII, consistent with metastatic deposit in a 72-year-old male patient with history of parotid carcinoma

Fig. 2.22 Axial contrast-enhanced CT demonstrating multiple hypoenhancing liver lesions (*arrows*), representing metastases in a 33-year-old male with history of testicular germ cell tumor

Fig. 2.23 Axial Contrast-enhanced CT image demonstrating multiple enhancing lesions (*arrows*) compatible with metastatic carcinoid in a 72-year old woman with carcinoid

more conspicuous on the interstitial phase [50]. In some cases, the hypoenhancing metastases can only be seen in the early enhancing phases as area of hypoenhancement compared to the enhancing liver background parenchyma; they then become isoenhancing with the liver parenchyma in delayed interstitial phase of contrast (Fig. 2.22).

- As previously described (under cystic lesions), metastases can appear cystic or necrotic with a resultant high signal intensity on T2-weighted images with no significant enhancement on various postgadolinium phases, and ovarian cancer metastases and post-treatment metastases are the main avascular metastases. Avascular metastases can be misdiagnosed as a simple cyst but can be differentiated through detection of the indistinct margins in the interstitial phase and size reduction of the metastases due to peripheral enhancement, while the simple cysts remain unenhanced and unchanged in size with well-defined borders [50].
- Hyperenhancing Metastases: Metastases can enhance greater than the liver parenchyma. Common primary tumors leading to this pattern are neuroendocrine tumors, renal cell carcinoma, thyroid, melanoma, and breast. These tumors can demonstrate increased enhancement on arterial phases of postcontrast CT and MRI [51], with washout in the delayed phase; these features help to differentiate them from the flash-filling hemangioma (which retain contrast in delayed phase (Fig. 2.23).
- MRI (with its various pulse sequences) can help differentiate malignant from benign lesions. On routine T2 weighted images (TE around 90 ms), benign lesions (such as cysts and hemangions) demonstrate markedly increased signal intensity, as opposed to malignant lesions (such as metastases) which demonstrate mildly or moderately increased signal intensity. On heavily T2 weighted images (TE >160 ms), benign lesions demonstrate further increase in signal intensity, as opposed to malignant lesions which demonstrate less signal intensity and can appear isointense to the surrounding liver, may not be conspicuous and could be missed [50].

Teaching Points

Metastases can exhibit various morphologic and enhancement patterns. The nature of primary tumor plays a key role in the pattern of enhancement of metastases. Thus, metastases can be considered in the differential diagnosis of various patterns.

Hypovascular Hepatocellular Carcinoma

Hepatocellular carcinoma will be discussed under the category of arterially enhancing lesions as HCC most commonly manifests as arterially enhancing mass. However, hepatocellular can rarely appear as a hypovascular mass (Fig. 2.24).

Peripheral Washout Sign

The "peripheral washout sign" was reported in delayed 10-min postgadolinium MR images and appears as peripheral hypointense rim relative to the relatively enhancing center of the lesion (Fig 2.25) [47]. Peripheral washout sign indicates malignancy and has been described in some cases of hepatic metastases from carcinoid, breast, colon, and gastric cancers. Although this has been described in a 10-min delay after IV contrast administration on MRI, we are more frequently observing this pattern in standard delayed techniques and also on CT scan examinations.

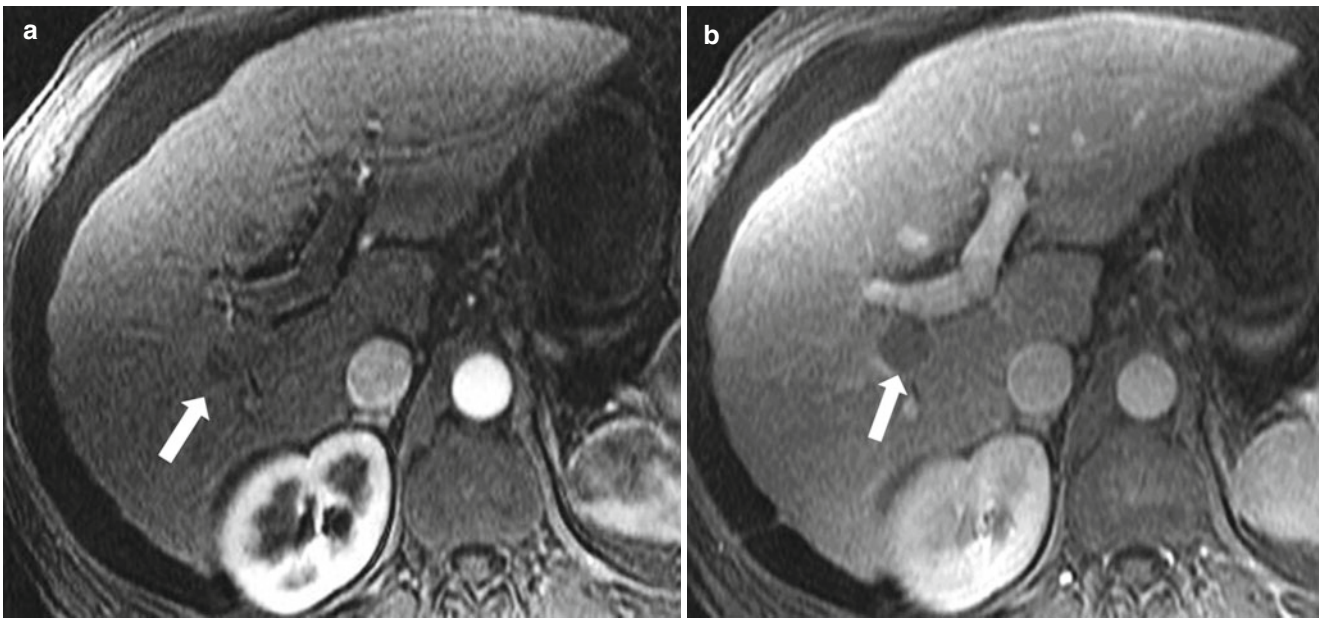

Fig. 2.24 Hypovascular HCC. Axial contrast enhanced T1-weighted images in arterial phase (**a**) and venous phase (**b**), demonstrating a single focus of hypoenhancement (*arrow*) which becomes more conspicuous in venous phase within the posterior segment of the right hepatic lobe, this was pathologically proven to represent HCC

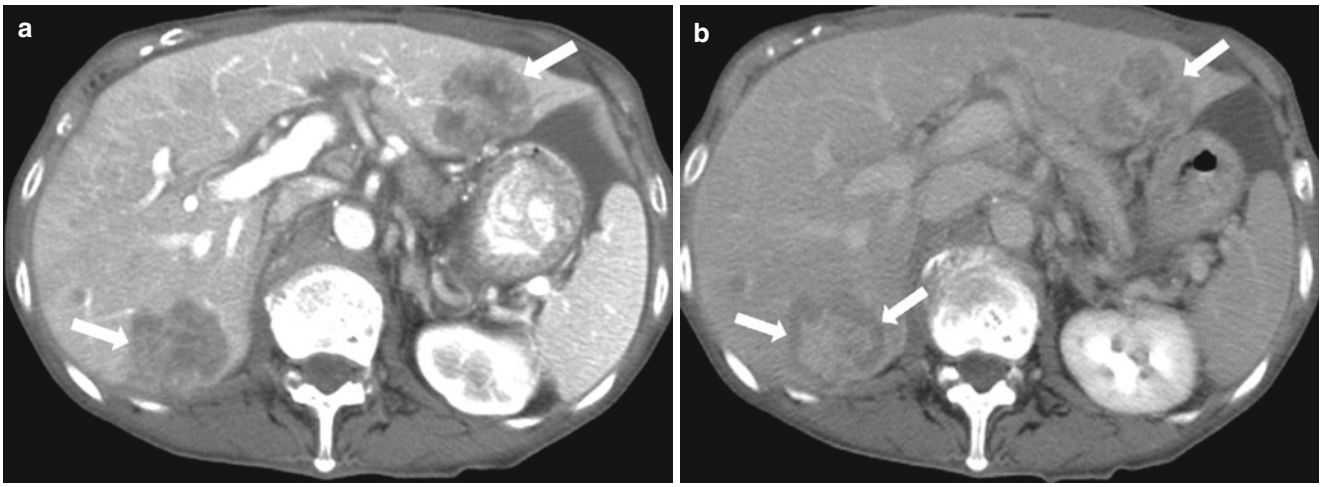

Fig. 2.25 Peripheral washout sign. Axial contrast enhanced CT in arterial phase (**a**), and delayed phase (**b**) demonstrate hypoattenuating lesions (*arrows in* **a**), with a peripheral hypoattenuating rim in delayed phase (*arrow in* **b**), consistent with metastatic deposits secondary to colon adenocarcinoma

Key Teaching Point

The main differential diagnoses for arterially enhancing lesions include hepatocellular carcinoma, focal nodular hyperplasia, adenoma, flash-filling hemangioma, and metastases. In the presence of cirrhotic features, HCC is the most likely diagnosis particularly when supported by enhancement washout and pseudocapsule in delayed phase. In the absence of cirrhosis, benign entities are more likely. Flash-filling hemangioma is specifically characterized by retention of contrast in delayed phase and increased signal intensity on T2-weighted image. In younger women of childbearing age, with history of oral contraceptive use, adenoma is the likely diagnosis. Central scar is present in about 50–70 % of cases of FNH. Pseudolesions are rarer but can mimic other more common diagnoses mentioned above.

Arterial-Phase Enhancing Lesions (Algorithm 2.5)

These lesions demonstrate increased enhancement compared to the liver parenchyma on arterial phase after intravenous contrast administration:

- Hepatocellular carcinoma
- Focal nodular hyperplasia
- Flash-filling hemangioma
- Hepatocellular adenoma
- Hyperenhancing metastases

Other less common causes of arterially enhancing lesions/pseudolesions:

- AVF/AVM
- THID/THAD
- Aberrant gastric venous drainage
- Hot spot sign
- Angiosarcoma
- Nodular regenerative hyperplasia
- Inflammatory pseudotumor

Algorithm 2.5 The main differential diagnostic possibilities for arterially enhancing lesions are hepatocellular carcinoma (particularly in cirrhosis), focal nodular hyperplasia, fash filling hemangioma, adenoma and metastases. The clinical context and constellation of findings on other phases of enhancement and pulse sequences are helpful in reaching specific diagnosis. Rdiologists should be aware of the other rarer lesions (such as LRN) and pseudolesions (such as THID, AGVD and hot spot sign) which may mimic more aggressive pathologies

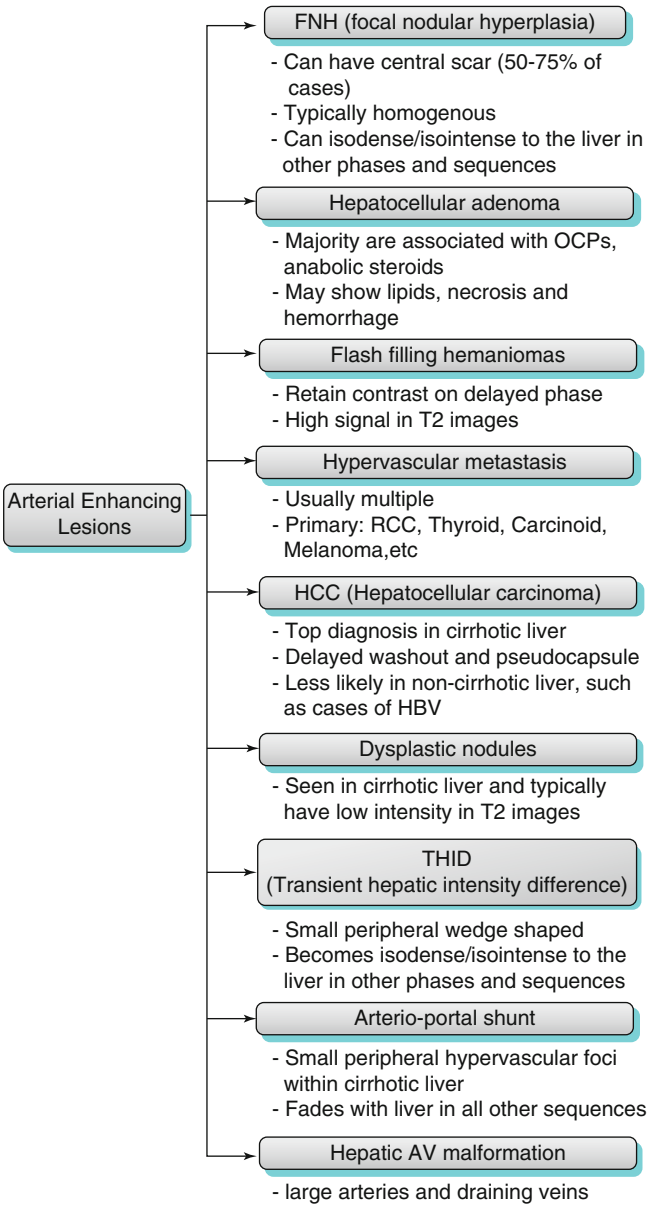

Hepatocellular Carcinoma (HCC)

HCC is considered the most common primary hepatic malignancy. The incidence is higher in cirrhotic liver as compared to the non-cirrhotic liver with hepatitis B is the major risk factor in the non-cirrhotic liver [52].

HCC is three times more common in men than women [53]. The difference in the 5-year survival rate for untreated symptomatic HCC in contrast to the survival rate in cirrhotic patients with small (<2 cm) HCC who have undergone liver transplantation is very impressive (5 and 80 %, respectively). This highlights the importance of early detection and treatment of HCC [52].

The pathogenesis of HCC begins with the development of benign regenerative nodules which in turn transform to dysplastic nodule. Dysplastic nodule is a premalignant lesion that finally progress to HCC [54].

MRI is better than CT in detection and characterization of HCC due to its superior contrast resolution, multiplanar imaging, and the ability to obtain serial dynamic imaging after IV administration of contrast using various pulse sequences. The combined use of all these features helps in superior characterization of hepatic nodules/masses and reaches a definitive diagnosis [55].

Larger HCCs >2 cm are more likely to follow the typical features of HCC, which have high signal intensity on T2-weighted images and low signal intensity on T1-weighted images with hyperenhancement on arterial phase and washout on delayed phase. The appearance of smaller HCCs <2 cm in MRI may vary as follows: on T2-weighted images, lesions may appear iso- to hyperintense to the surrounding liver, and on T1-weighted images, it is usually hypointense to the liver [55], and rarely HCC can contain high-protein content or less likely fat, which results in a high signal intensity on T1-weighted images.

The process of neoangiogenesis of HCC causes the specific features of HCC and renders the arterial phase of contrast-enhanced images to be the most sensitive sequence for detecting HCC [56], where the HCC shows moderate to intense enhancement in the early arterial postcontrast phase with gadolinium combined with washout on the delayed phase. These features are considered the only noninvasive

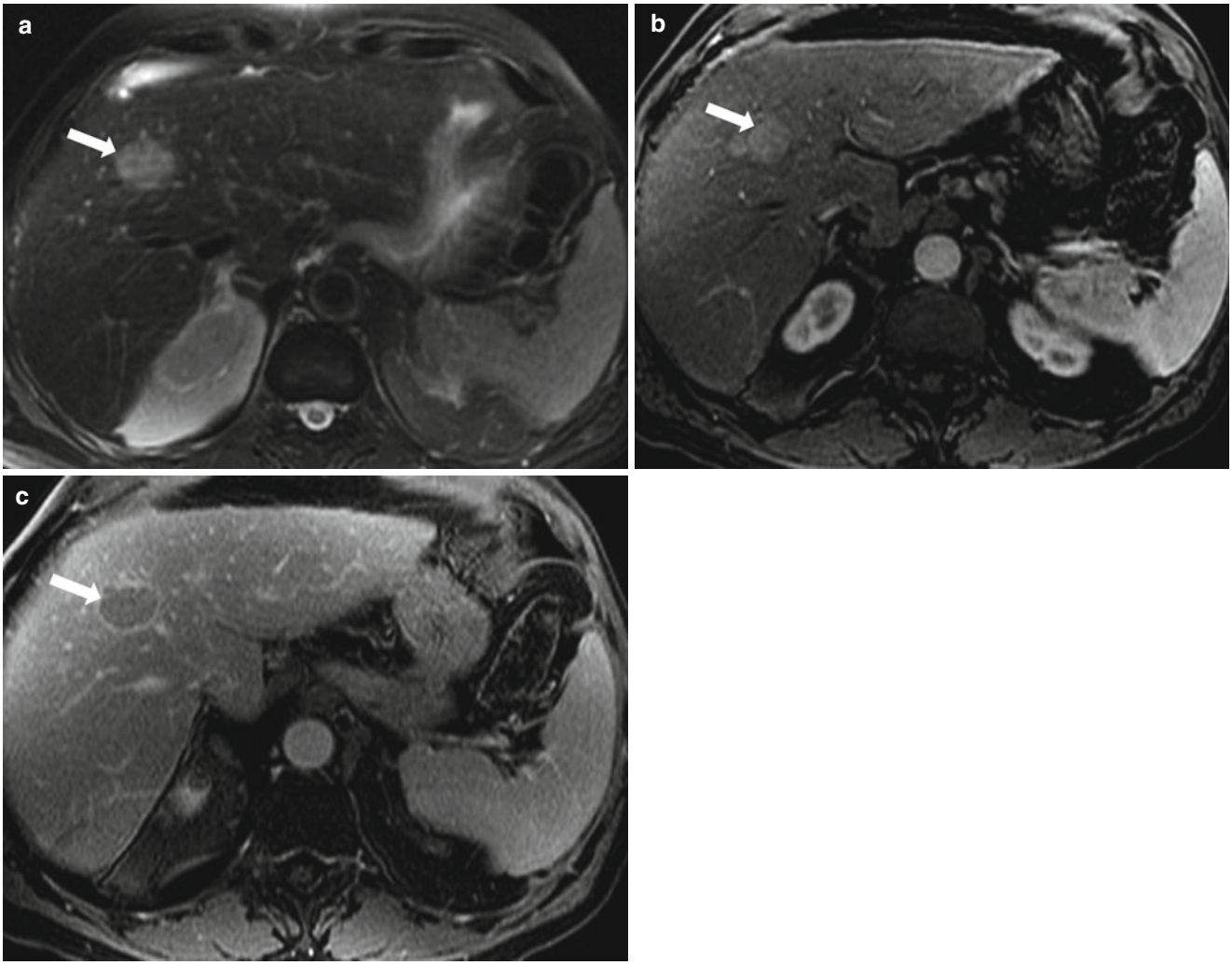

Fig. 2.26 HCC, axial fat-saturated T2-weighted image (**a**), axial contrast enhanced T1-weighted in arterial-phase (**b**) and delayed phase (**c**) demonstrate a focal lesion (*arrow*) exhibiting high signal intensity on T2-weighted image, homogeneous enhancement on arterial phase, and washout of enhancement as well as pseudocapsule (*arrow*) on delayed phase, consistent with hepatocellular carcinoma

radiological features in diagnosing HCC by the organization responsible for liver transplantation in the USA by the "United Network for Organ Sharing" {UNOS} [57]. Few HCC lesions are hypovascular and appear isointense with the liver parenchyma in the arterial postgadolinium phase, but show delayed washout in interstitial postgadolinium phase [58] (Fig. 2.26). This feature of delayed washout of the HCC can help in differentiating HCCs from other arterial enhancing lesions such s atypical hemangiomas (flash-filling hemangiomas), focal nodular hyperplasia, and hepatic adenomas.

Due to the development of the HCC from high-grade dysplastic nodules, there is an overlap between both entities. But there are some features that can be helpful in raising the suspicion of HCC over dysplastic nodules, such as development of new foci, larger size >2 cm, the presence of delayed enhancement washout, presence of a coexistent large HCC, and rapid interval growth of lesion (most reliable feature); while regression or disappearance of lesion on follow-up MR studies, small size of nodule <1.5 cm (in combination with the absence of a large coexistent HCC) is more consistent with dysplastic nodule.

Diffuse HCC occurs in 13 % of cases of HCC and appears as diffuse extensive heterogeneous permeative tumor often associated with portal vein thrombosis. These tumors appear as heterogeneous mottled moderate low signal intensity on T1-weighted images and moderate high signal intensity on T2-weighted images. These features are nonspecific and limit the ability of noncontrast sequences in detecting rather diagnosing the diffuse disease due to the similarity with the hepatic background. These tumors have patchy or nodular early enhancement pattern with enhancement washout and pseudocapsule enhancement on delayed phase [59].

Venous thrombosis associated with HCC is almost always affecting the portal veins. However, it can involve the hepatic veins. Tumor thrombosis is commonly high signal in T2-weighted images and enhances with gadolinium, in contrast to bland thrombus which appears hypointense in T2-weighted images and does not enhance with gadolinium

[59]. On diffusion-weighted image, tumor thrombus demonstrates restricted diffusion, in contrast to bland thrombus which does not restrict diffusion.

Hepatocellular Adenoma

Hepatocellular adenomas (HCAs) are monoclonal hepatocellular benign epithelial neoplasms. Typically, 90 % of adenomas are described in young women with history of oral contraceptive [60]. Tumors typically involute spontaneously after patients withdraw from birth control pills. Other much less frequent associations include the use of anabolic steroids and disorders associated with abnormal carbohydrate metabolism [61]. Patients may present with a variety of symptoms, most commonly right upper quadrant abdominal pain, which is mostly related to hemorrhage into the tumor in 30 % of cases, and 10 % of adenomas transform into malignancy [62].

The histological hallmark consists of clusters of benign hepatocytes arranged in slender plates of cells. Neoplastic hepatocytes are separated by slit-like sinusoids and numerous thin-walled veins. Bile ducts are absent in internal structure of hepatocellular adenoma [63]. The typical MR appearance of adenoma is homogeneously mild hyperintensity on T2-weighted images. On T1-weighted images, homogeneously mild hypointensity, isointensity, or hyperintensity are described (Fig. 2.27). On postcontrast CT and MR images, homogeneous blush immediately after contrast has been described which uniformly fades to isodensity/isointensity relative to the liver parenchyma in the delayed phase. Some adenomas contain intracellular lipid yielding a drop in signal intensity on out-of-phase compared to in-phase pulse sequences.

Recently, hepatocellular adenomas have been classified into four subtypes (Table 2.2): hepatocyte nuclear factor-1α-mutated HCAs (HNF-HCAs), HCAs characterized by β-catenin mutations, inflammatory HCAs (I-HCAs), and miscellaneous category, which are due to different gene mutations. They have different pathological features which impact their features on imaging, the I-HCAs are the most

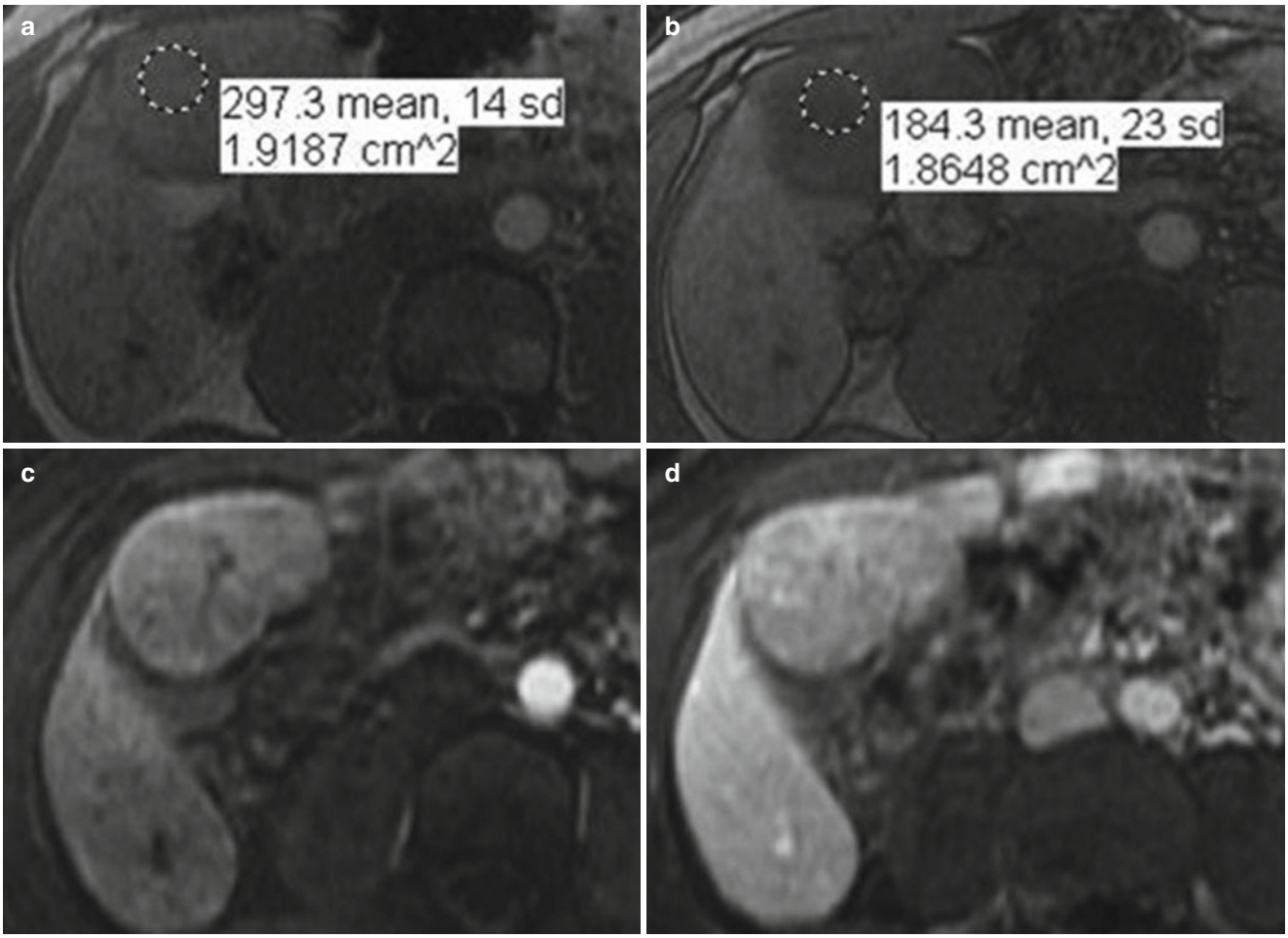

Fig. 2.27 Hepatocellular adenoma. Axial in-phase (**a**), and out-of-phase (**b**) demonstrating a well circumscribed mass (*arrow*), exhibiting homogeneous drop of signal on out-of-phase compared to in-phase secondary to the presence of intracellular lipid (microscopic fat), consistent with adenoma. Axial contrast enhanced T1-weighted images in arterial phase (**c**) and delayed phase (**d**) in a different patient demonstrating masses (*arrows*) exhibiting slight homogeneous enhancement in arterial phase and washout on delayed phase. Image courtesy, Christine Menias, Mayo Clinic, Arizona

Table 2.2 Classification of hepatocellular adenoma [64, 65]

Type	Incidence (%)	Symptoms	Malignant transformation	Hemorrhage
Inflammatory	40–50	Young female, history of OCP and obese Chronic anemia Systemic inflammatory syndrome: fever, ↑WBC, ↑CRP	10 % show increased risk of malignancy	20–25 % Tumors >5 cm (the highest risk of bleeding: 30 %)
HNF-1alpha mutated	30–35	Asymptomatic, discovered incidentally	Minimal or no risk	Tumors<5 cm show minimal risk of bleeding
B-catenin mutated	10–15	Asymptomatic, but can be occasionally symptomatic if bleeds	5–10 %	Has a risk of bleeding, exact incidence is unknown

Table 2.3 MR imaging features of hepatocellular adenomas [64, 65]

Type	T1-WI	T2-WI	Chemical shift	Arterial phase	Venous and delayed phase
Inflammatory	Isointense or mildly ↑	↑ signal	No signal drop	Intense enhancement	Persistent enhancement
HNF-1alpha mutated	Isointense or ↑	Intense to slightly ↑	Intracellular lipid content → signal drop	Moderate enhancement	Enhancement doesn't persist
B-catenin mutated	Nonspecific	Nonspecific	Nonspecific	Marked enhancement	Possible washout

common subtype and account for about 40–50 % of all hepatocellular adenomas, this typically appears hyperintense on T2-weighted images with intense arterial enhancement that persist in the venous and delayed phases, while the HNF-HCAs represent the second most common type of hepatocellular adenoma and constitute about 30–35 % of all hepatocellular adenomas and show diffuse steatosis which appears as homogeneous high signal in T1-weighted images with moderate arterial enhancement that does not persist into the venous phase, and lastly the HCAs with β-catenin have no specific features and generally shows arterial enhancement with portal venous washout, which make it very difficult to distinguish from HCC [64, 65] (Table 2.3).

Dysplastic Nodules

Dysplastic nodules represent intermediate step in the pathway of carcinogenesis of hepatocytes in cirrhotic liver. These are considered as premalignant nodules and are found in about 20 % of cirrhotic livers. Some studies have documented the development of HCC within a dysplastic nodule in few months. Dysplastic nodules appear most commonly as isointense or hypointense on T2-weighted images and isointense to hyperintense on T1-weighted images [66]. Unlike regenerative nodules, dysplastic nodules have been found to contain isolated arteries, with documented correlation between the extent of enhancement on arterial phase and the grade of dysplastic nodules; the greater the degree of arterial enhancement of the nodule, the more likely the potential of malignant transformation of HCC [67]. However, dysplastic nodules have the tendency to fade toward background signal of the liver in the interstitial and delayed phase of enhancement, which help in its differentiation from the small HCC which are most likely to exhibit enhancement washout with delayed capsule enhancement. Other features that can help differentiate dysplastic nodules from HCC include: high signal intensity of HCC on T2-weighted images. Foci of small HCC, which develop in the high-grade dysplastic nodules, appear as high signal intensity foci within low signal intensity nodule on T2-weighted images (nodule within a nodule sign) [68].

Focal Nodular Hyperplasia

Focal nodular hyperplasia (FNH) is an uncommon lesion defined by localized area of hepatic cell hyperplasia within the normal liver. FNH is developmental in origin and predominantly is found in women during the third to fifth decades of life; however, they can appear in any age group and both sexes, and FNH tends to show progressive involution after the fifth decade of life and has no direct association with oral contraceptive use [69]. No malignant potential has been described for FNH. The most common appearance on MR images ranges from isointensity to mild hyperintensity on T2-weighted images and iso- to mild hypointensity on T1-weighted images (Fig. 2.28). FNH typically enhances with an intense uniform blush on immediate postgadolinium images and fades rapidly to almost isointensity (typically at 1 min after contrast). Commonly, small (<1.5 cm) FNH is isointense on all precontrast images and may be appreciated only on the immediate postgadolinium images. Approximately two thirds of FNH >3 cm have a central scar which is noted on CT to demonstrate low attenuation. On MR, central scar demonstrates high signal intensity on T2-weighted images as a characteristic feature of FNH [69]. The central scar exhibits lack of enhancement on immediate postcontrast CT and MR images, and the majority shows gradual enhancement in the delayed phase. Central scar is less common in small FNH (seen in approximately 50 %). However, larger lesions tend to demonstrate a lobulated

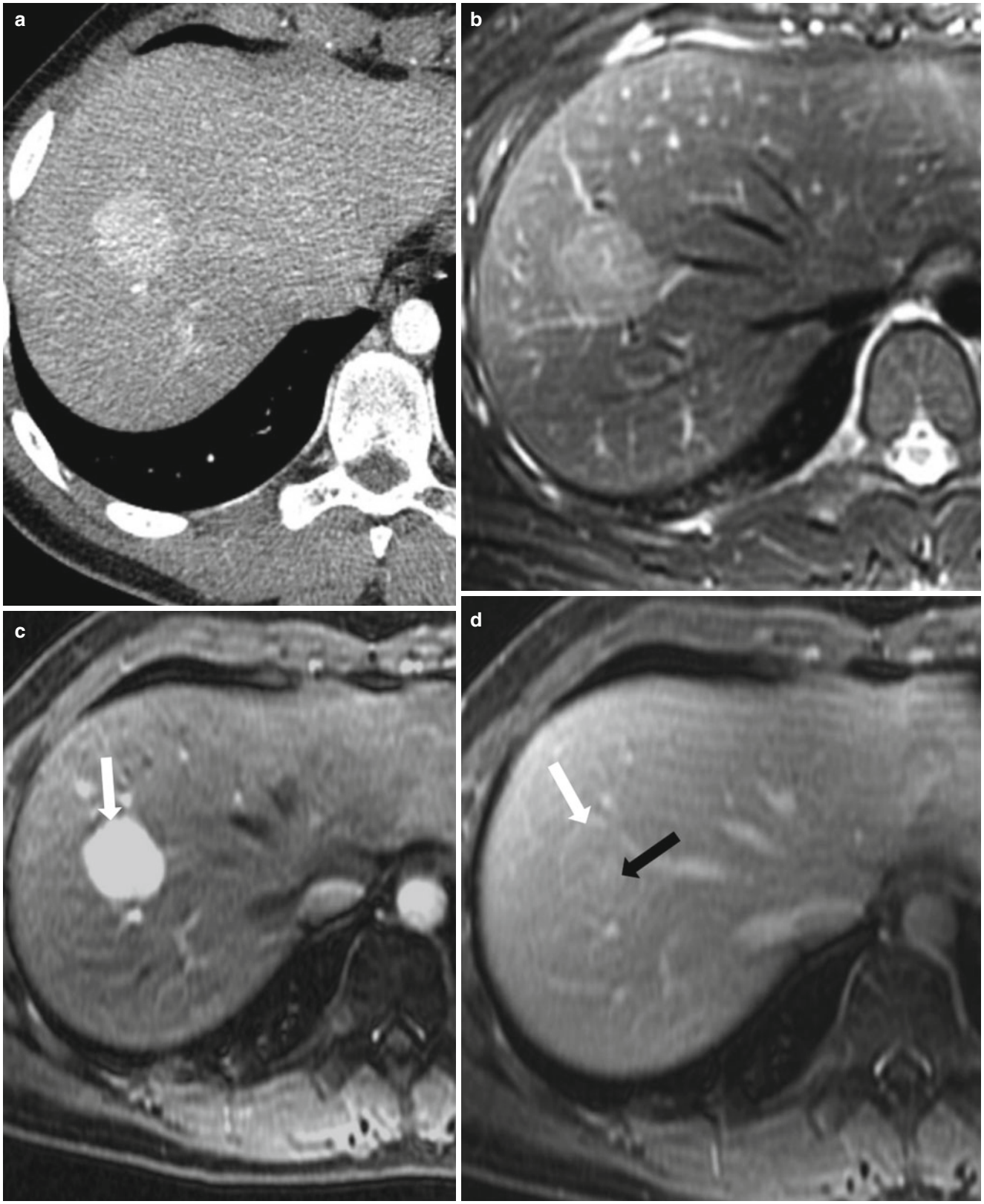

Fig. 2.28 FNH. Contrast-enhanced CT showing arterial homogeneous enhancement of the FNH (**a**). T2-weighted image (**b**) showing high signal of the lesion with higher signal central scar (*arrow*). Early (**c**) and delayed (**d**) postcontrast 3D GRE T1-weighted images demonstrate early intense enhancement with delayed isoenhancement compared to the liver parenchyma with enhancing scar in the delayed phase

contour that is rarely seen in malignant lesions. Small FNHs (which do not have central scar) may be difficult to characterize and can be confused for other enhancing benign and malignant lesions. Fatty infiltration of FNH is rare and only sporadically mentioned in the literature [70, 71].

Other lesions demonstrating arterial-phase enhancement are discussed elsewhere in this chapter, such as flash-filling hemangioma (Fig. 2.29, discussed with hemangioma under delayed enhancement) and hyperenhancing metastases (Fig. 2.23, discussed earlier under metastases).

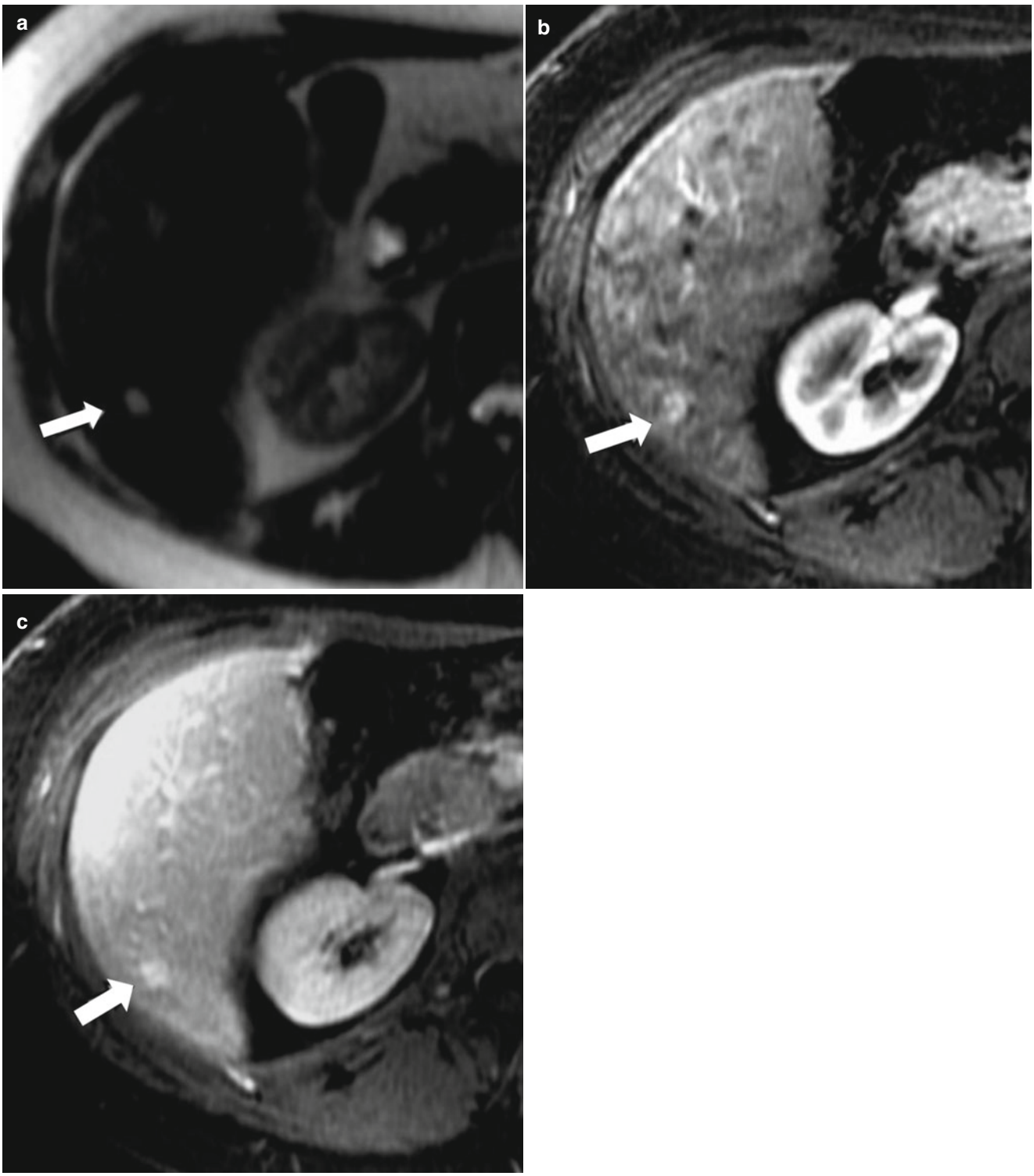

Fig. 2.29 Flash-filling hemangioma. Axial non-fat-saturated T2-weighted image (**a**), axial arterial and delayed phases contrast enhanced T1-weighted images (**b**, **c**), showing a well circumscribed small lesion (*arrow*) exhibiting homogeneous enhancement on arterial phase with retention of contrast on delayed-phase and markedly increased signal intensity on T2-weighted image

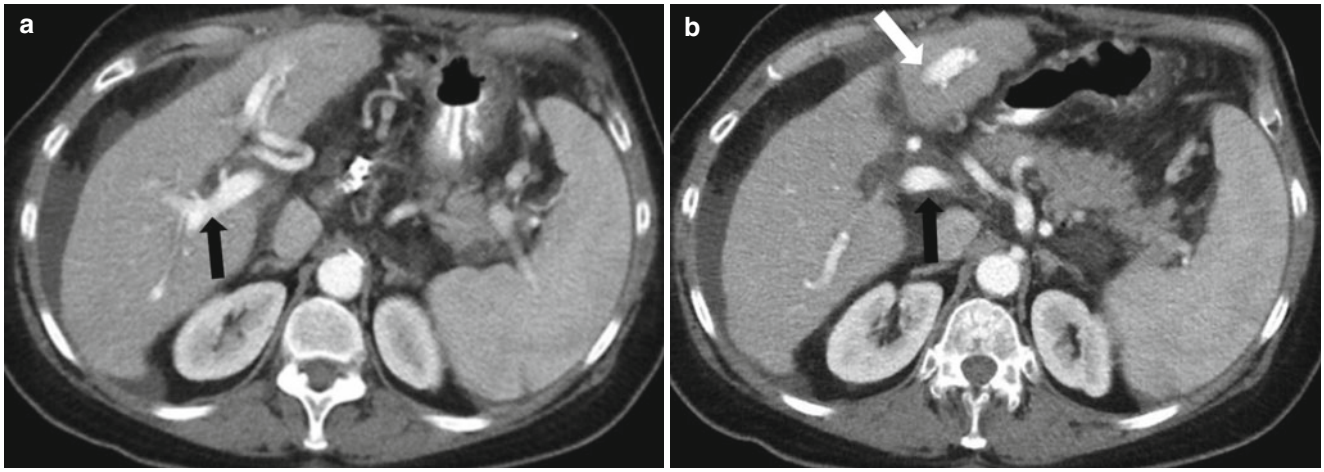

Fig. 2.30 Arteriovenous fistula. Axial contrast enhanced CT in arterial phase (**a**, **b**) demonstrating a linear enhancing lesion within the left hapatic lobe (*white arrow*) representing AV fistula in the left hepatic lobe, with early filling of the portal vein (*black arrow*) in the arterial phase

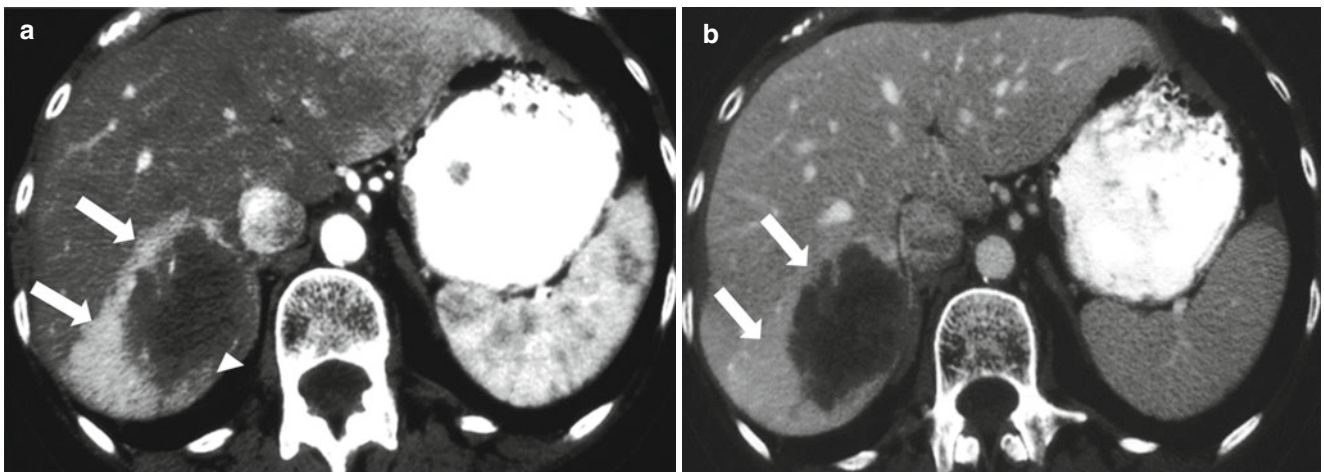

Fig. 2.31 Transient hepatic attenuation difference. Axial contrast-enhanced CT in arterial phase (**a**) and venous phase (**b**), showing a wedge-shaped enhancing area (*arrows*) in arterial that fades away on subsequent portal-phase image. This is caused by a hypoattenuating colon metastasis (*arrowhead*) occluding a small portal vein branch. Image courtesy, Isaac R. Francis, University of Michigan, Ann Arbor

Arteriovenous Fistulas

Arteriovenous communication or fistula is defined as an abnormal connection between the hepatic artery and portal vein. It can be either acquired or congenital. Acquired causes can result from liver injury by tumor, trauma, or iatrogenic causes such as a complication to percutaneous liver biopsy. On MRI, arteriovenous fistula can be visualized as signal void serpiginous structures which enhance after IV gadolinium administration as dilation of the afferent and efferent vessels or early enhancement of the efferent vessel. The presence of early filling of the vein and transient parenchymal enhancement in the watershed distribution may direct attention to it (Fig. 2.30) [72, 73].

Congenital arteriovenous fistulas are rare. An example of this is hereditary hemorrhagic telangiectasia where there are telangiectatic lesions in the skin and mucous membrane as well as multiple arteriovenous fistula in the liver, lung, and CNS. The liver shows multiple variable-sized enhancing lesions that follow the enhancement of the hepatic arteries.

THAD/THID (Transient Hepatic Attenuation/ Intensity Difference)

THID in MR images are the equivalent of THAD in CT, which are wedge-shaped areas of parenchymal enhancement visible only in the hepatic artery phase (Fig. 2.31) and caused by compensatory arterial hyperperfusion when portal flow decreases. This may be due to many causes leading to communication among the vessels, sinusoids, and venules that open in response to autonomic nervous system and humoral factors activated by the liver demands for oxygen and metabolites. Portal venous occlusion is also a cause for THADs.

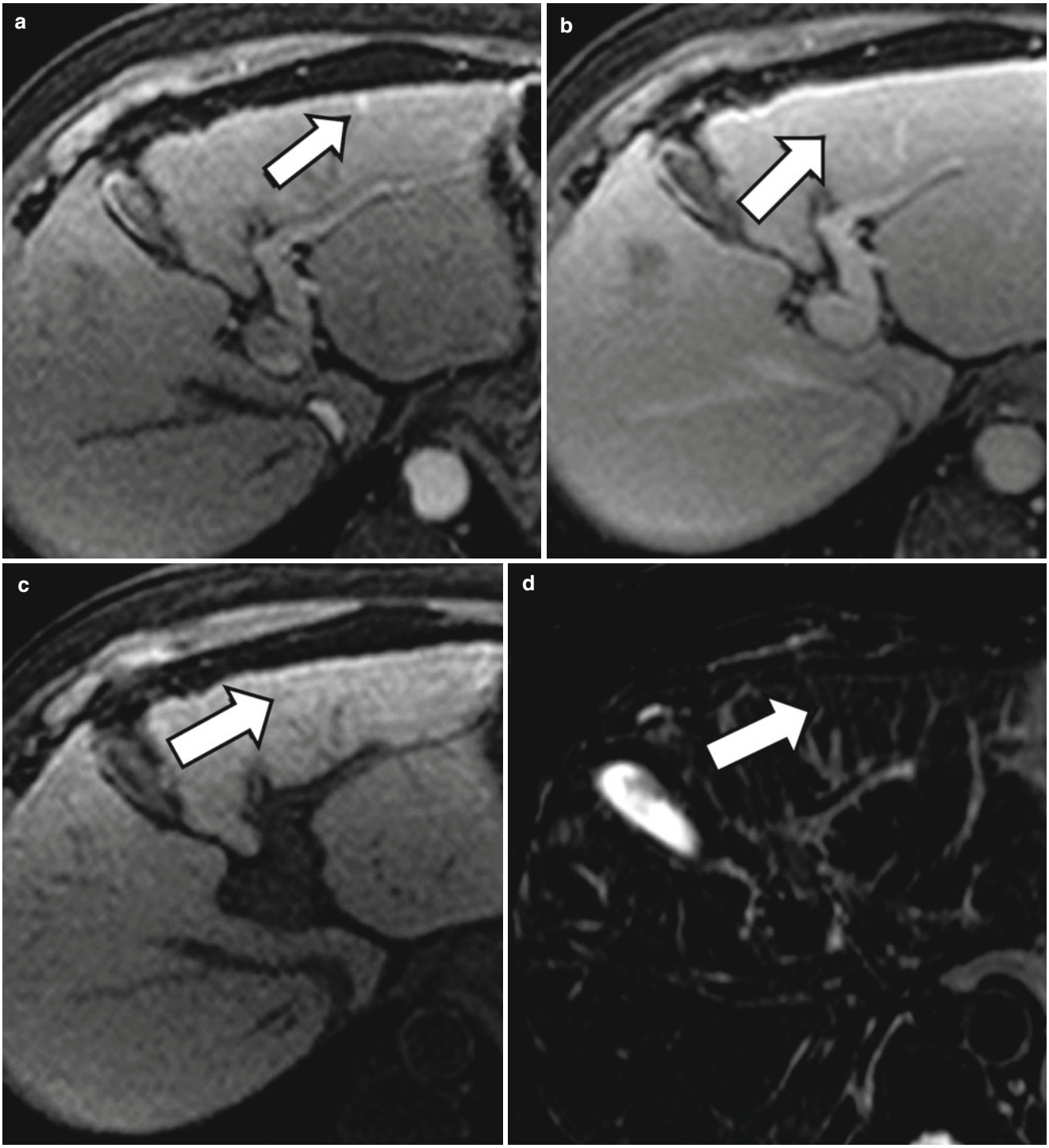

Fig. 2.32 THID, axial contrast enhanced T1-weighted in arterial phase (**a**), venous phase (**b**), axial nonenhanced T1-weighted (**c**) and axial T2-weighted (**d**) showing an enhancing focus visible only in arterial phase with no corresponding signal abnormality (*arrow*) in delayed phase, nonenhanced T1-weighted or T2-weighted images, representing transient hepatic intensity difference

They usually appear as small peripheral wedge-shaped areas of arterial hyperenhancement and fade within the liver parenchyma in all other sequences (Fig. 2.32). Most of these are idiopathic. However, some of THID are associated with other focal lesions that may occlude branches of the portal vein and lead to this phenomenon in a segmental distribution [74]. The arterioportal shunt has the same appearance as the THAD/THID and however different pathogenesis.